JOURNAL OF GEOPHYSICAL RESEARCH, VOL. 87, NO. C10, PAGES 7903–7924, SEPTEMBER 20, 1982

The Flux and Mixing Rates of Antarctic Bottom Water Within the North Atlantic

J. A. WHITEHEAD, JR. AND L. V. WORTHINGTON

Woods Hole Oceanographic Institution, Woods Hole, Massachusetts 02543

Calculation was made of the northward flow of Antarctic Bottom Water into the western North Atlantic Basin through a passageway approximately 300 km wide between the Ceara Rise and the Mid-Atlantic Ridge at about 4°N. Two moorings carrying four current meters each were placed in the region where currents were expected to be the greatest and were left for 360 days. The current was not steady, but exhibited large surges with approximately a 60-day time scale whose cause is unknown. Current meters in the fastest flowing region all exhibited a net northward flow. It is estimated that approximately 0.8×10^6 m^3 s^{-1} of water colder than 1.9°C (potential temperature) flowed on the average into the North Atlantic, with this number possibly being too small by 0.3×10^6 m^3 s^{-1} or too big by 0.1×10^6 m^3 s^{-1} depending upon estimates of the width of the region, which the current meters sample. However, these numbers differ from geostrophic estimates of 1.98×10^6 m^3 s^{-1}, the disagreement coming almost entirely from the fact that the geostrophic estimates give a sizeable flux of water colder than 1.2°C while the current meters do not. Based upon the two different flux rates, residence times and mixing coefficients are calculated for Antarctic Bottom Water for each 0.1°C potential temperature interval from 1.0°C to 1.9°C. Finally, some comments on the dynamics of the northward flow are made.

1. INTRODUCTION

In his great treatise on the stratosphere of the Atlantic Ocean, *Wüst* [1935, 1978] presented meridional sections of temperature, salinity, dissolved oxygen, and density (σ_t). These sections provided the first adequate description of the Atlantic water masses and clearly distinguished those formed in the North Atlantic from those formed in the Southern Ocean. On the western side of the Atlantic three water masses dominate: Antarctic Intermediate Water that extends northward across the equator to 20°N above 1000 m, North Atlantic Deep Water that extends southward as far as 40°S between 1500 m and 4000 m, and, below this, Antarctic Bottom Water that occupies the greatest depths in the western North and South Atlantic.

It should not be supposed that much of the 'Antarctic Bottom Water' in the western North Atlantic was actually formed in the Southern Ocean. Water at 1.9° (in this paper, all temperatures are potential temperatures) in the North American Basin has a salinity of ~ 34.9‰. Water of this salinity must consist almost wholly of North Atlantic Deep Water with only the faintest tinge of pure Antarctic Bottom Water. (A similar statement applies to the saline Mediterranean water at mid-depths in the North Atlantic, even where it is so diluted as to be barely distinguishable from western North Atlantic Water.) *Worthington* [1981] has remarked that none of the fine-scale classes in his world ocean volumetric census is common both to the Southern Ocean (Atlantic) and the North Atlantic; water of Antarctic origin is modified by mixing with North Atlantic Deep Water well south of the equator. Nevertheless, we will use the term 'Antarctic Bottom Water' because it has been hallowed by long usage and because the contribution from Antarctica becomes stronger with decreasing temperature.

A more or less meridional deep water section from Antarctica through the western basins of the South Atlantic into the North American Basin can be seen in Figure 1. As water colder than 1.8° crosses the equator, it encounters the Ceara Abyssal Plain, which stretches from approximately 1°N to 4°N and is very flat, being between 4400 and 4500 m deep except for occasional isolated topographic hills. At approximately 4°N, the topography becomes rougher and more seamounts are found. The deepest bottom is now approximately 4600 m but it is unclear whether the deep regions here channel directly to the deeper North Atlantic basin or not. The passage here is approximately 300 km wide and is bounded on the west by the Ceara Rise and on the east by the Mid-Atlantic Ridge (see Figure 2). Further north the Antarctic Bottom Water is encountered at depths greater than 4500 m. The ocean floor from the equator to roughly 4°N thus acts as a gigantic dam to Antarctic Bottom Water, and only water at depths of 4500 m or less (or water that can be carried up to those depths) can continue northward. We formed a partnership to investigate this flux. One of us (JAW) was primarily interested in seeing whether the simple hydraulic models of strait flows [*Whitehead et al.*, 1974; *Gill*, 1977] are useful or whether other processes predominate as suggested, for instance, by *Rydberg* [1980]. The other (LVW) wished to determine the gross amount of Antarctic Bottom Water entering the North Atlantic and thus to estimate its residence time. We believe that moored current meters can give estimates of mass flux through such topographic passages with errors that are small by oceanographic standards (i.e., to the order of tens of percent error).

Our basic tools were two CTDs, eight current meters, and related equipment. Our first task was to use a CTD to help us decide where to deploy the current meters. We left Barbados in R/V *Oceanus* on November 25, 1977, and steamed southeastward to the Ceara Rise, a protrusion that narrows the channel between the Brazilian continental slope and the mid-Atlantic Ridge. We made a CTD section (Figure 3) from the Ceara Rise in a northeasterly direction to the Mid-Atlantic Ridge. (See Figure 2 for the location of sections referred to hereinafter.) The temperature profile for this section can be seen in Figure 3. Antarctic Bottom Water (<1.9°) occupies

Paper number 2C0759.
0148-0227/82/002C-0759$05.00

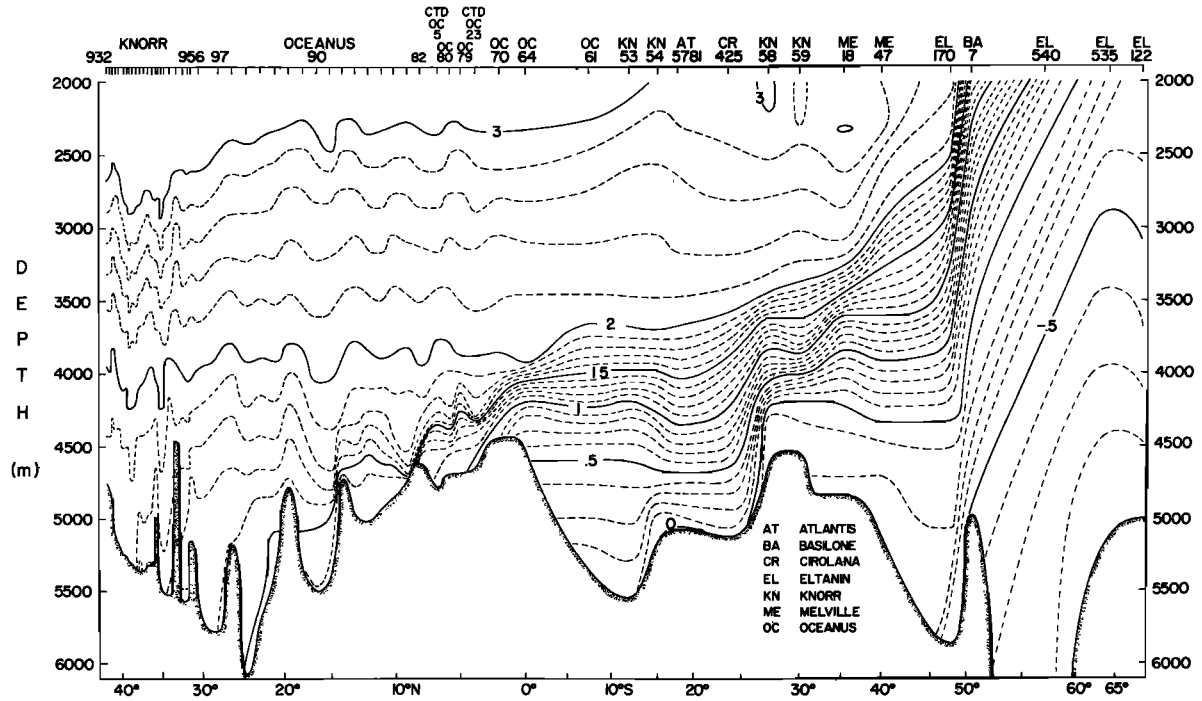

Fig. 1. Approximate north-south section of potential temperature along the deepest portion of the western Atlantic Basin.

the greatest depths. There is a nearly isothermal layer at about 1.1°. Above this is a relatively strong thermocline between 1.2° and 1.8°. North Atlantic Deep Water, specifically that of the deep western boundary current lies above the Antarctic Bottom Water; it flows southward, hugging the continental slope. The slope of the deepest isotherms (assuming that there was a zero-velocity surface immediately below the Atlantic Deep Water) indicated a more or less even northward flow of Antarctic Bottom Water from the Ceara Rise to the Mid-Atlantic Ridge. (Since the potential temperature/salinity relationship remains virtually constant in Antarctic Bottom Water, the slopes of these deep isotherms closely approximate the slopes of deep isopycnals.)

After completing this section (we had the misfortune to lose a CTD and rosette on station 9) we steamed to the western slope of the Mid-Atlantic Ridge at 4°N, and made another CTD section running due west from the ridge to the Ceara Rise. In this section (Figure 4), the topography was more irregular than that of the 6°N section. The slope of the deep isotherms, associated with the northward flow of Antarctic Bottom Water, was rather gentle until the western edge of the section was reached when it steepened abruptly. We decided to deploy our eight current meters (Figure 4) amid the steeply sloping isotherms in such a way as to sample the velocity of the water column between 1.0° and 1.9°.

The current meters were anchored on two low (~300 m) hills near the base of the Ceara Rise, in the region where the deep isotherms had the strongest slope. The current meters were equipped with temperature recorders, which enabled us to keep track of the hydrographic conditions at the mooring site for the duration of the experiment. After we launched the current meters on December 8, 1977, *Oceanus* returned to Woods Hole.

The following November we sailed from Recife, Brazil, and made a hydrographic section (Figure 5), which cut across the equator at 45° from the Brazilian continental margin to the Romanch Fracture. We then made a zonal hydrographic section (Figure 6) across the Antarctic Bottom Water at 2°N with an additional dogleg northward at approximately 40°40'W to close off the section to the Ceara Rise. After completing that section we returned to the launch site and recovered both moorings. We then made three additional hydrographic stations near the site. After this we steamed in a northwesterly direction to 16°N 55°W in order to track the Antarctic Bottom Water as it descends into the North American Basin. Thence we steamed northward, making hydrographic stations until we joined a previous N/S hydro-

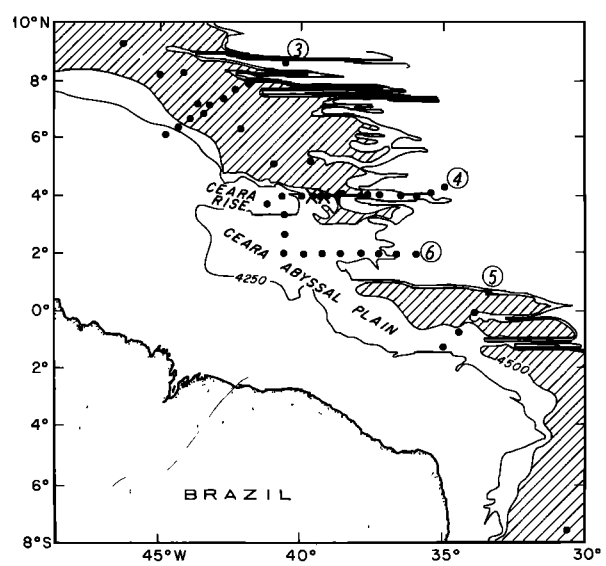

Fig. 2. Location of stations (dots) and moorings (crosses). The 4250- and 4500-m depth contours, based upon the map by *Moody et al.* [1979] are drawn in. The numbers refer to figure numbers for temperature sections.

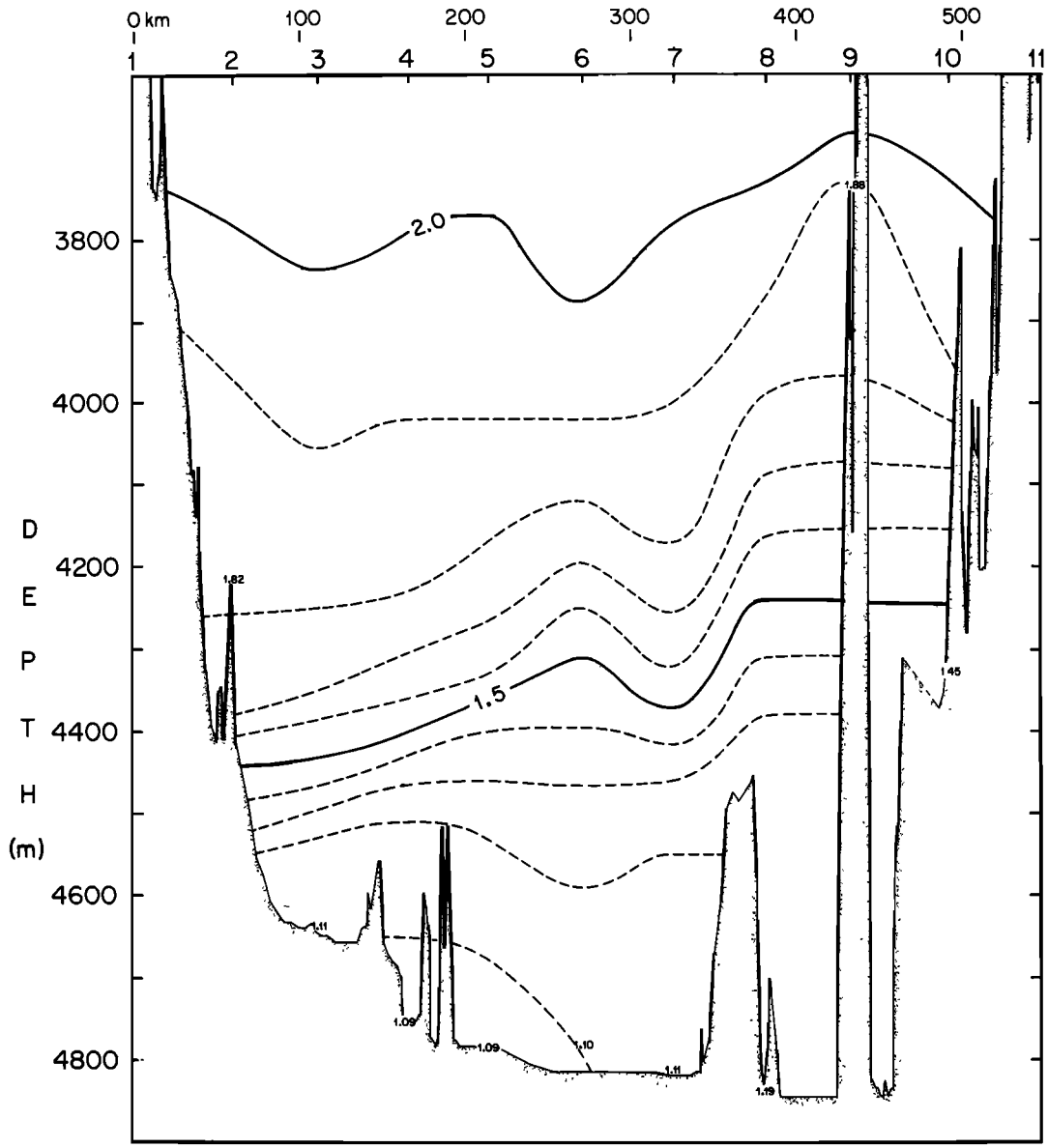

Fig. 3. Section across the western North Atlantic Basin (location shown in Figure 2) from approximately 6°N 45°W to 9°N 40°30'W. Southwest is to the left.

graphic section made in October 1976 in connection with the POLYMODE experiment [*McCartney et al.*, 1980]. All the stations north of the equator shown in Figure 1 are from this experiment and the POLYMODE section.

Properties of the Water

Temperature sections. The four sections shown in Figures 3–6 enable one to trace the changes in depth of the isotherms as one travels northward. Starting in the section that crosses the equator (Figure 5), there is a sharp transition to Antarctic Bottom Water at approximately 4000 m depth, and although the temperature decreases all the way to the bottom, the gradient is most pronounced between 4000 and 4300 m. In the section at 2°N, which doglegs up to the Ceara Rise on the left-hand side (Figure 6), one can see there is again a fairly sharp transition to Antarctic Bottom Water. There is some evidence for an eastward current at depth greater than 4000 m on the left-hand side. At 4°N (Figure 4), the Antarctic Bottom Water is deeper on the left-hand side of the passage by up to 300 m and has far less slope on the right-hand side. The properties of the water right next to the bottom differ little from the properties of the water right next to the bottom at 2°N. Finally, in the northernmost section (Figure 3), at approximately 8°N, greatest slopes of the isotherms are found mainly on the right-hand (northeast) side of the passage and at somewhat greater depths. The bottom waters are now somewhat warmer than those in the sections further south.

The entire picture is consistent with Antarctic Bottom Water being skimmed northward at depths from 4000 to 4500 m into the North Atlantic Basin, where it then flows downward as a density current toward the right-hand side of the North Atlantic Basin.

Current meter observations. The above picture could have been sketched with considerably less detail from historical data alone. Therefore, one of our central purposes was to augment this picture with direct current measurements in the place where currents might be strongest. Our

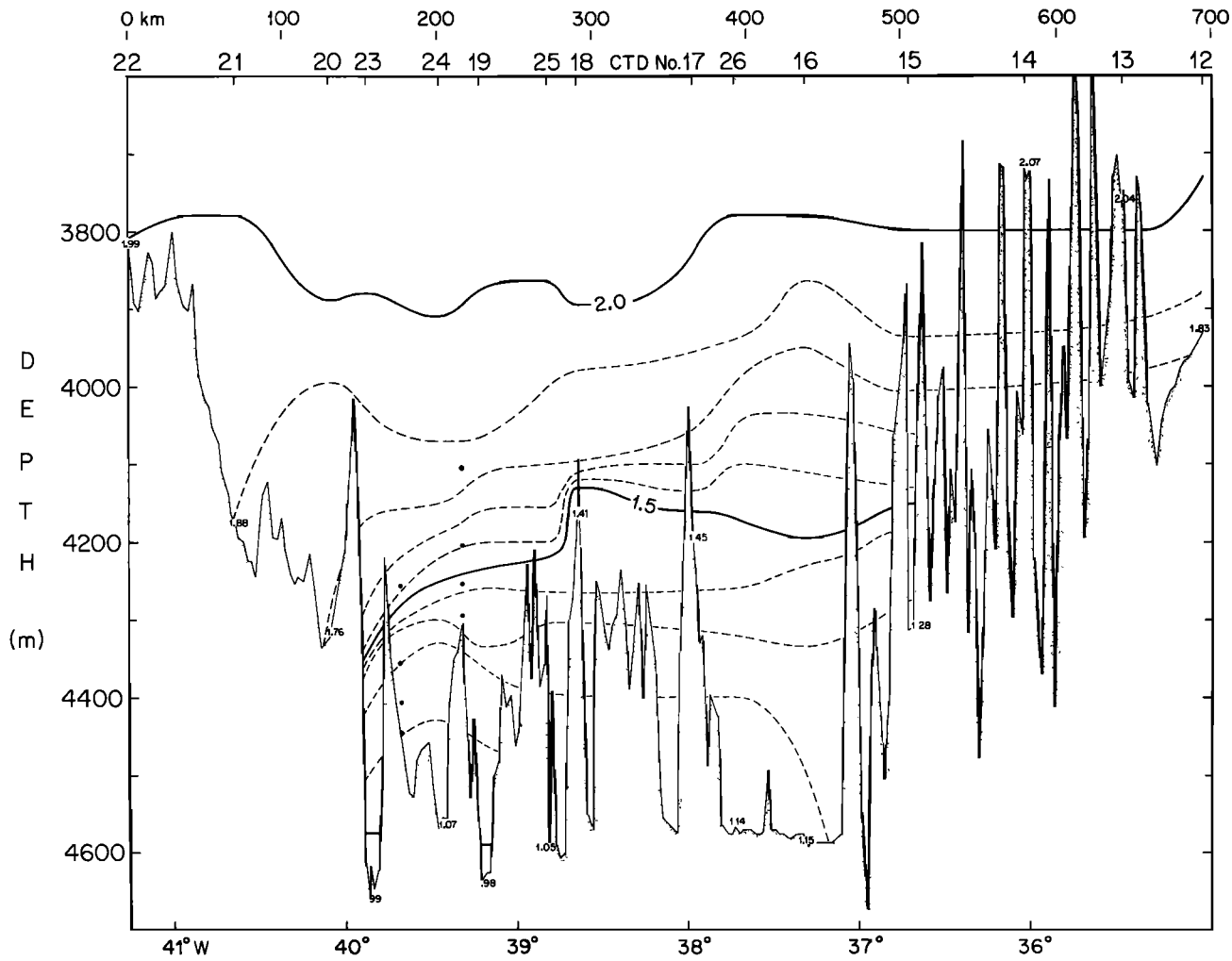

Fig. 4. Section across the western Atlantic Basin (location shown in Figure 2) at 4°N from the Ceara Rise on the left to the Mid-Atlantic Ridge on the right. The eight dots are the locations of the current meters.

strategy was to locate the moorings as close to the 'crest' of the passageway between the North and South Atlantic as possible. In such a location the currents would be 'controlled' by topography and hence strongly contained in the vertical and horizontal. We do not mean 'controlled' to be taken strictly in the hydraulic sense—such processes as turbulence and friction may play an important role in the dynamics of the real ocean currents—but rather we mean 'controlled' to mean strongly influenced by topography. Thus, the currents are controlled in that if topography were changed (a very unlikely event in present day physical oceanography) the speed, shape, and location of the currents would change. Upon the basis of the observations and our knowledge of the topography, two moorings containing vector averaging current meters each were deployed at 4°2.5'N, 39°40.5'W, and 4°1.3'N, 39°19.0'W. The meters were placed at depths of 10, 50, 100, and 200 m above the bottom and recorded current speed and direction along with temperature from December 10, 1977, to December 4, 1978; readings were taken every 15 min.

The steady component of the observed currents are discussed in section 2. An estimate of the mean northward flow of water at 0.1°C intervals is made along with an estimate and discussion of possible errors. This is then compared with an estimate of velocity from the density field by using geostrophic methods. It is found that the two methods exhibit close agreement (to within 20%) in the volume flux for waters warmer than 1.2°C, but exhibit more than an order of magnitude disagreement for waters between 1.0° and 1.2°C. The origin of this remarkable disagreement is unclear.

Next, in section 3, the residence times, 'eddy' fluxes, and upward (cross isotherm) advection rates consistent with these fluxes and known volumes of water for each 0.1° interval in the North Atlantic are calculated. These are done subject to the assumption that the flux is stationary for climatological time scales appropriate for these waters in the North Atlantic. The numbers are found to be very sensitive to the large disagreement between the current meter and geostrophic estimates for flux of water colder than 1.2°C, but the numbers obtained are believed to bracket the true values. Finally, in section 4, features of the time dependent component of the flows is presented, accompanied by remarks and questions on the possible dynamics in the control region.

2. Mean Northward Transport

Figure 7 shows progressive vector diagrams for the eight current meters. The data shown here and used in the computations to be described next were subjected to a Gaussian filter with a 1-day half width to eliminate the tidal signal. Ninety-five percent of the energy of greater than a 5-day period is passed by this filter. All current meters

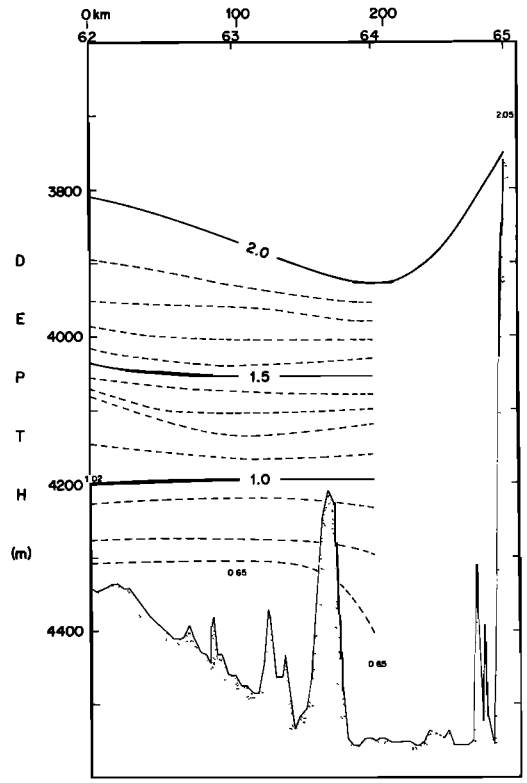

Fig. 5. Section across the equator in the western Atlantic (location shown in Figure 2) at approximately a 45° angle with the equator. Southwest is to the left.

demonstrate a net northward flux with the greatest flux in the east mooring. The bottom current meters exhibit a strong eastward velocity component whose cause is unknown (an Ekman layer flux would be toward the west). A veering to the right is consistent with flow over topography and both moorings were on topographic features.

Figure 8 shows stick diagrams of velocity and curves of potential temperature, speed, and direction for the eight current meters. Again the net northward flow was evident in most of the records, and two oscillatory periods of roughly 60 and 3 days are easy to see.

To calculate the volume transport as a function of the potential temperature, the average northward velocity and the average potential temperature over the 360-day record was calculated for the four current meters in each mooring and the values are shown in Table 1. The records were smoothed with a 5-day running mean to eliminate the three day oscillation. Table 1 also shows average eastward velocity, potential temperature, and a 'correction function' to be discussed later. Henceforth, u denotes eastward velocity and v denotes northward velocity. Mean northward velocity is plotted in Figure 9 as a function of depth. The transport of water near each mooring can be estimated by taking the area under a curve joining the velocity points. However, for purposes of conducting a volumetric census, transport will be estimated for water in each tenth of a degree temperature interval. One could do this by reading off velocity at temperatures of 1.95°, 1.85°, 1.75°C, etc. from Figure 9, which shows mean velocity and temperature in the current meters as a function of depth. This would be in error, however,

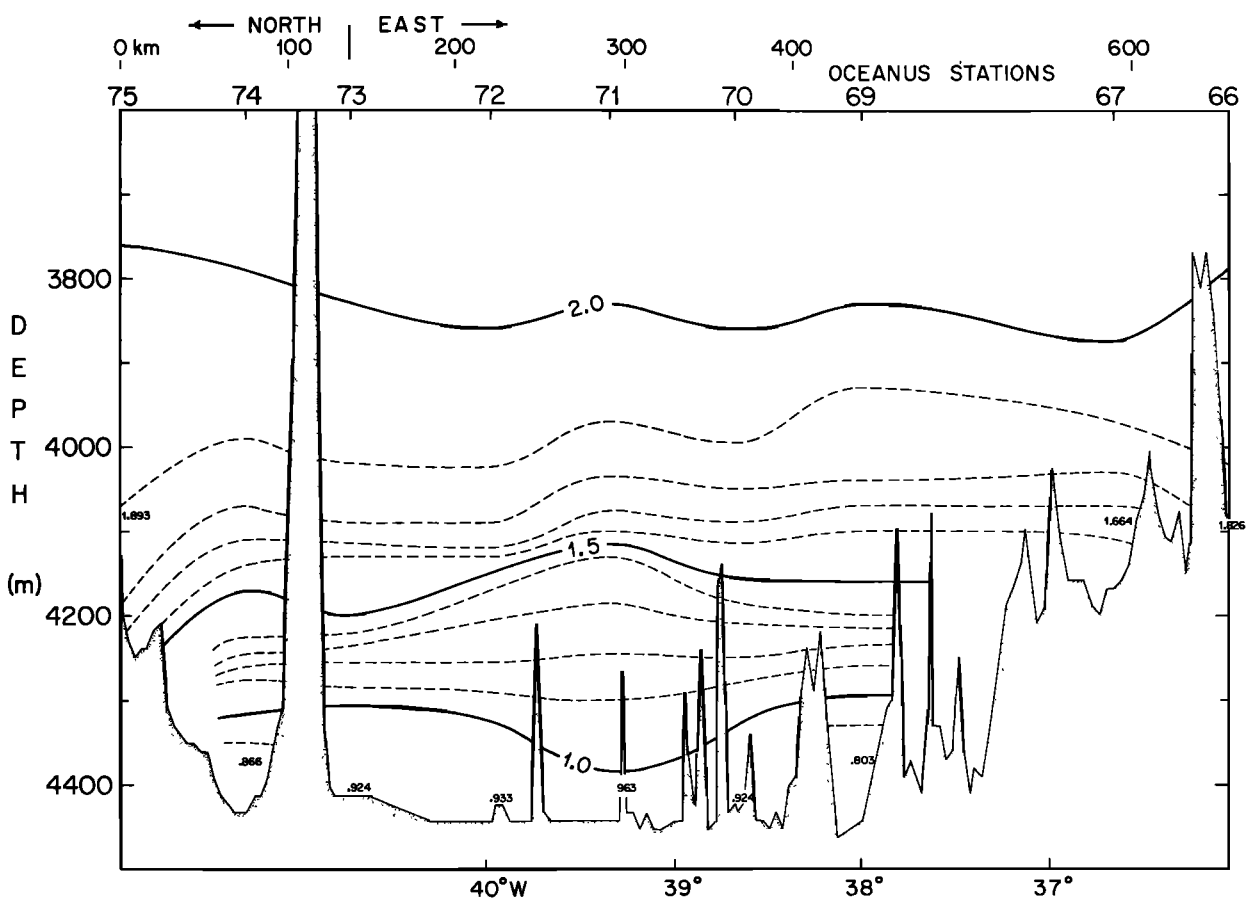

Fig. 6. Section across the western Atlantic (location shown in Figure 2) at 2°N from the flank of the Mid-Atlantic Ridge (over the Ceara Abyssal Plain) with a dogleg on the left up to the Ceara Rise.

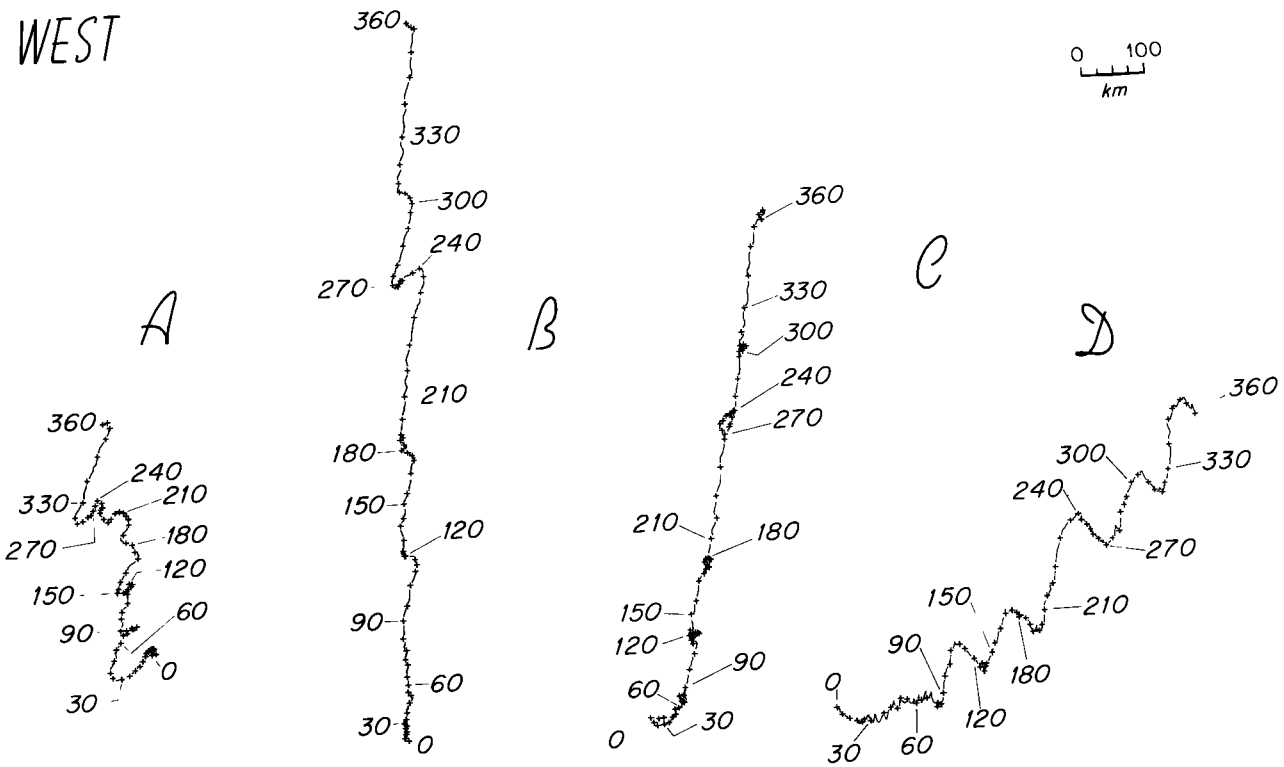

Fig. 7*a*

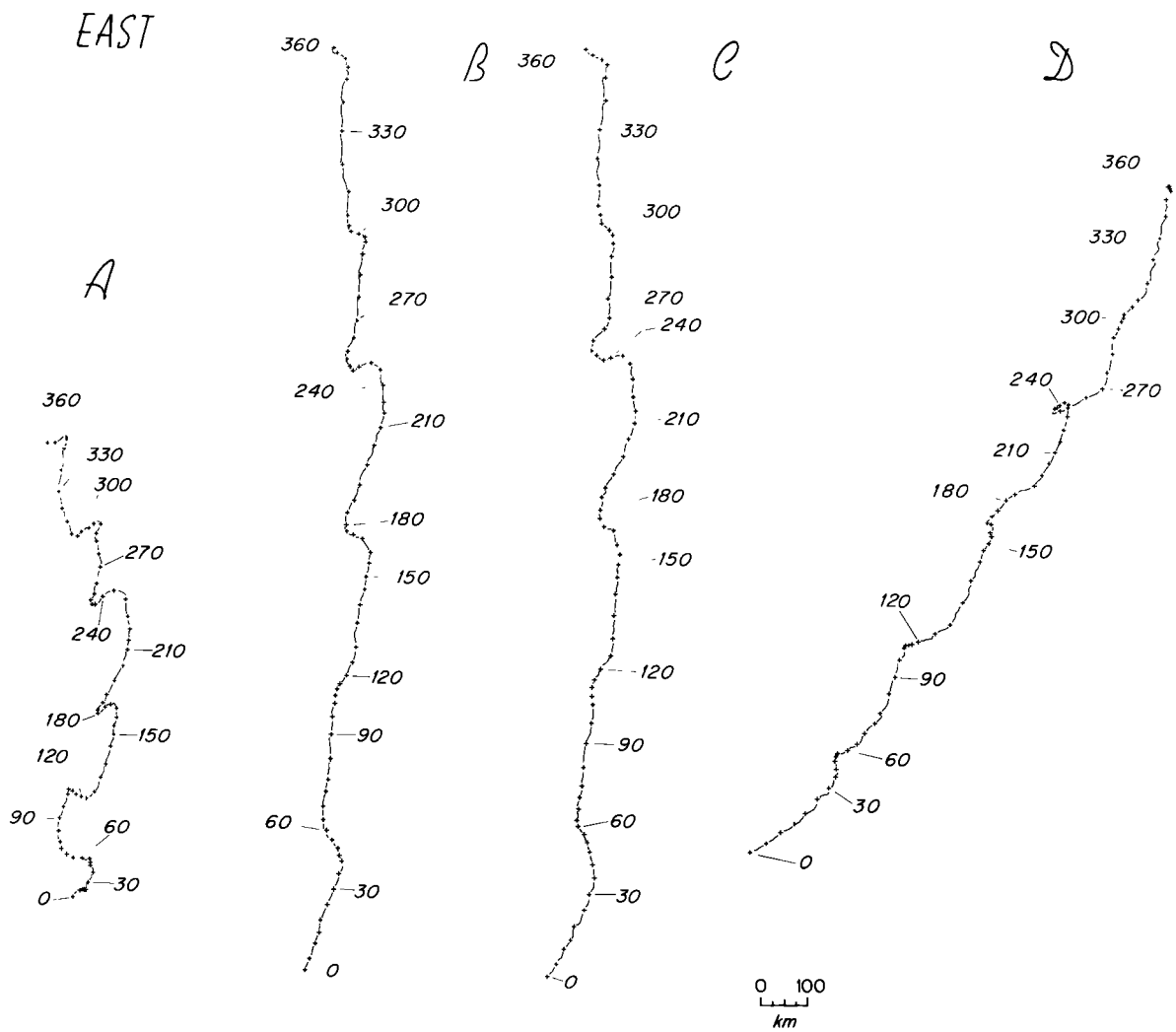

Fig. 7*b*

Fig. 7. Temperature, progressive vector diagrams, direction, and speed for the eight current meters. The west mooring data are at depths left to right of 4256, 4356, 4406, and 4446 m. The east mooring data are at depths of 4104, 4204, 4254, and 4294 m, respectively.

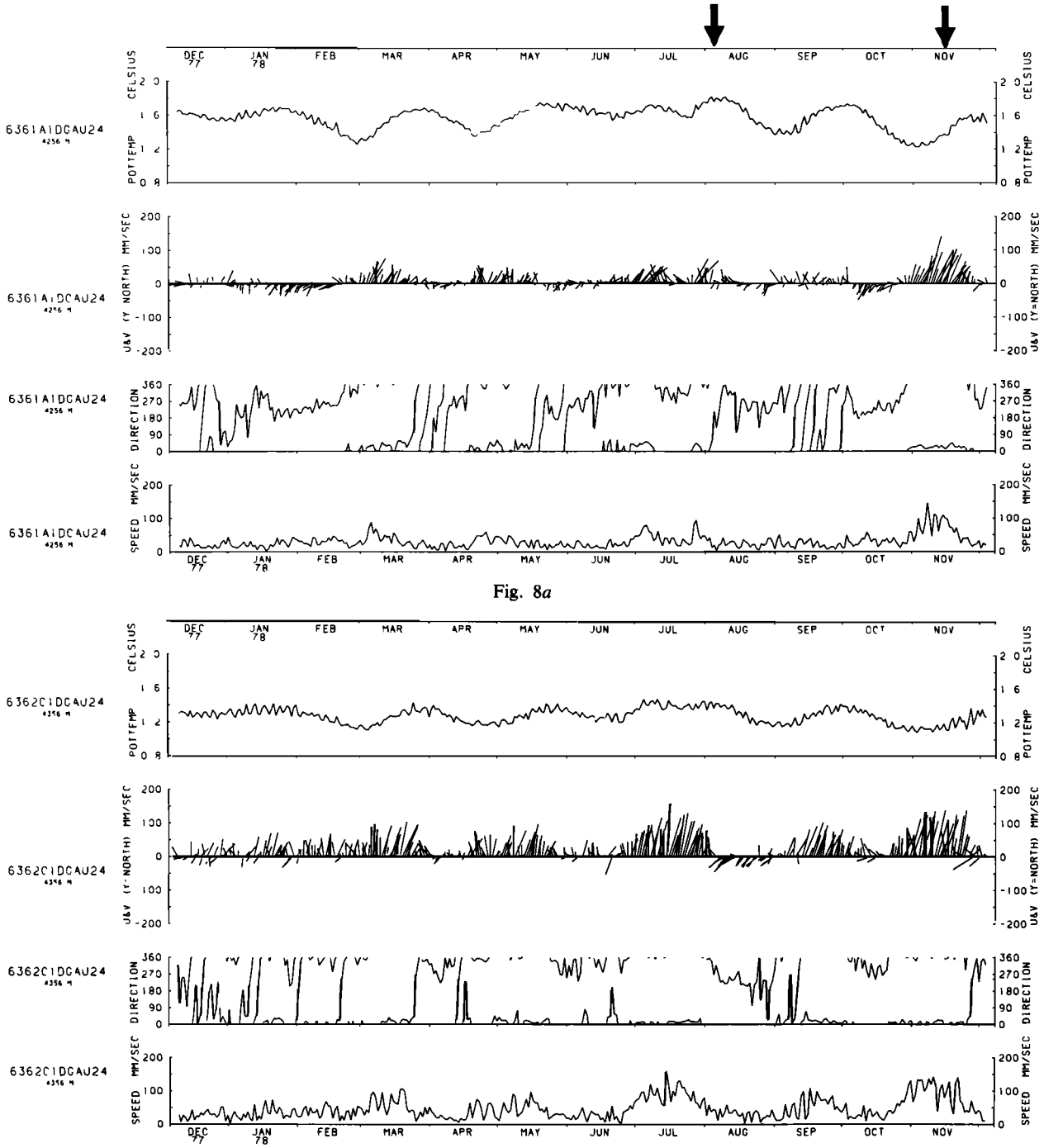

Fig. 8. Stick diagrams of velocity and curves of potential temperature, velocity, and direction from the current meter records. The sequence is the same as in Figure 7. The two arrows in the first record denote periods of slow (left) and fast (right) currents for estimates of Bernoulli potential as discussed in section 4 and given in Table 9.

because larger velocities occurred when water was colder, as can be easily seen by comparing the temperature records with the stick diagrams in Figure 8. (We have been assured by the mooring designers that a mooring this short in such currents would have negligible 'blow over.') This correspondence will be discussed more fully in section 4. The above curve would, in fact, be skewed by this process such that the warmer waters would be estimated to have a bigger volume flux than they really have, and the colder waters would have less. The total volume flux is proportional to the area under the velocity curve and would still be correctly determined. To correct for the skewing effect of the time-dependent flows, the average potential temperature at every depth was corrected by the value

$$\theta_c \equiv \frac{\overline{(v_i - \bar{v})(\theta_i - \bar{\theta})}}{360\,\bar{v}} \tag{1}$$

where subscript i refers to day number and the overbar here and in the rest of the article is a 360-day average of the daily average velocity, i.e.,

$$\frac{1}{360}\sum_{i=1}^{360}$$

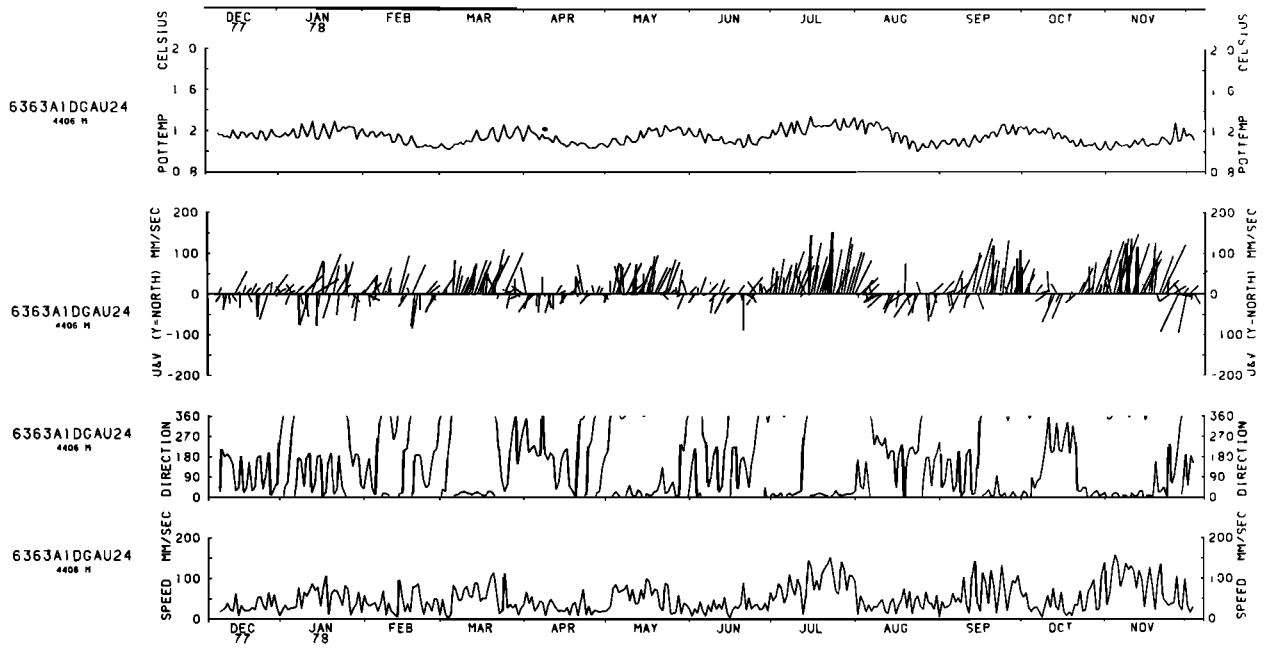

Fig. 8c

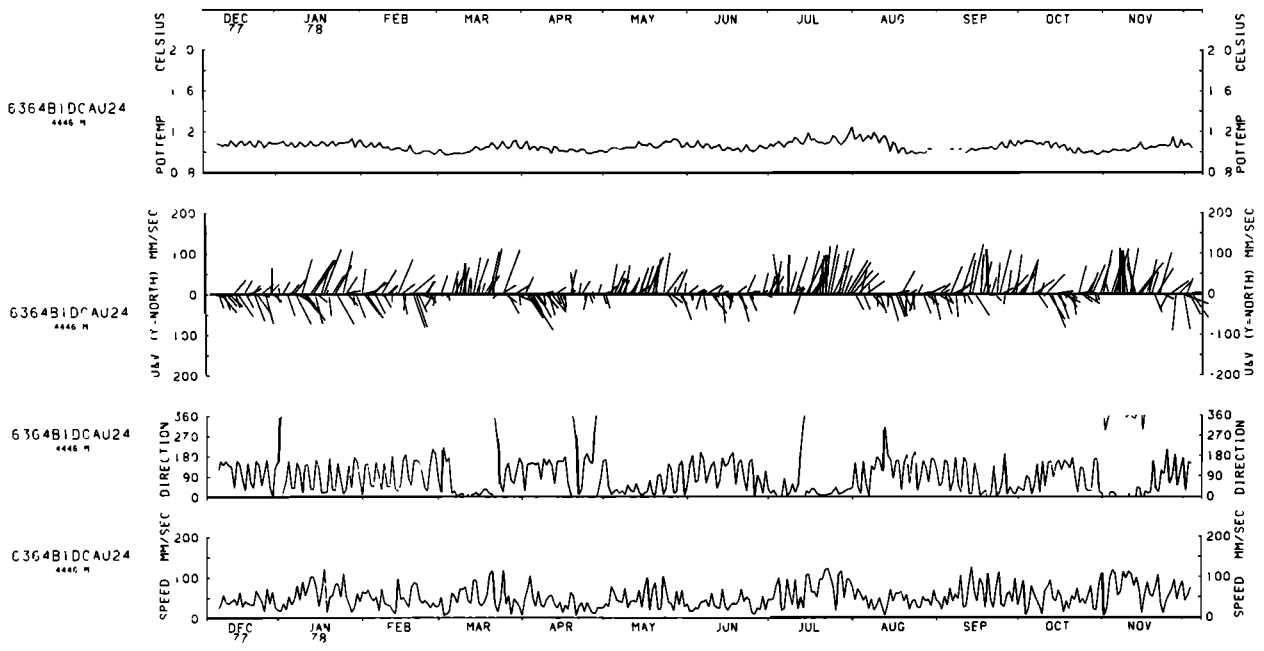

Fig. 8d

These corrections are listed in Table 1. Rationale for this correction is that the average flux of sensible heat (H relative to some arbitrary reference temperature) over a given period of time for water between depths z_1 and z_2 is equal to

$$H = w \int_{z_1}^{z_2} \rho C_p \overline{v\theta}\, dz$$

where w is some 'width' which the current meters are believed to be sampling, ρ is density, C_p is specific heat, v is northward velocity, and θ is temperature. If we separate mean and time varying flux, heat flux is

$$H = w \int_{z_1}^{z_2} \rho C_p \overline{(\bar{v} + v')(\bar{\theta} + \theta')} dz$$

Multiplying, we get

$$H = w \left[\int_{z_1}^{z_2} \rho C_p t\, \bar{v}\bar{\theta}\, dz + \int_{0z_1}^{tz_2} \rho C_p \overline{v'\theta'}\, dz\, dt \right]$$

and rearranging we get

$$H = w \int_{z_1}^{z_2} \rho C_p\, \bar{v} \left[\bar{\theta} + \frac{(v'\theta')}{v} \right] dz$$

Our 'correction temperature θ_c' is the term $\overline{v'\theta'}/\bar{v}$. It can be interpreted as an apparent change in potential temperature due to correlations between time dependent velocity and temperature.

The final points in temperature due to this correction and the velocity are shown in Figure 9 as solid circles for the

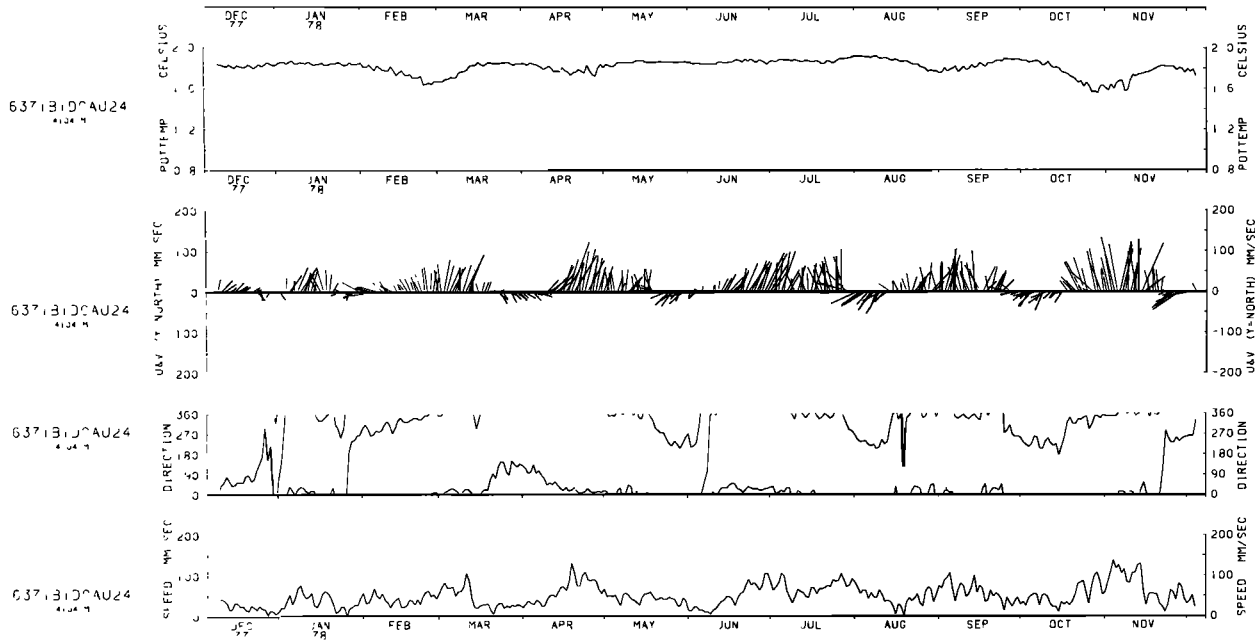

Fig. 8*e*

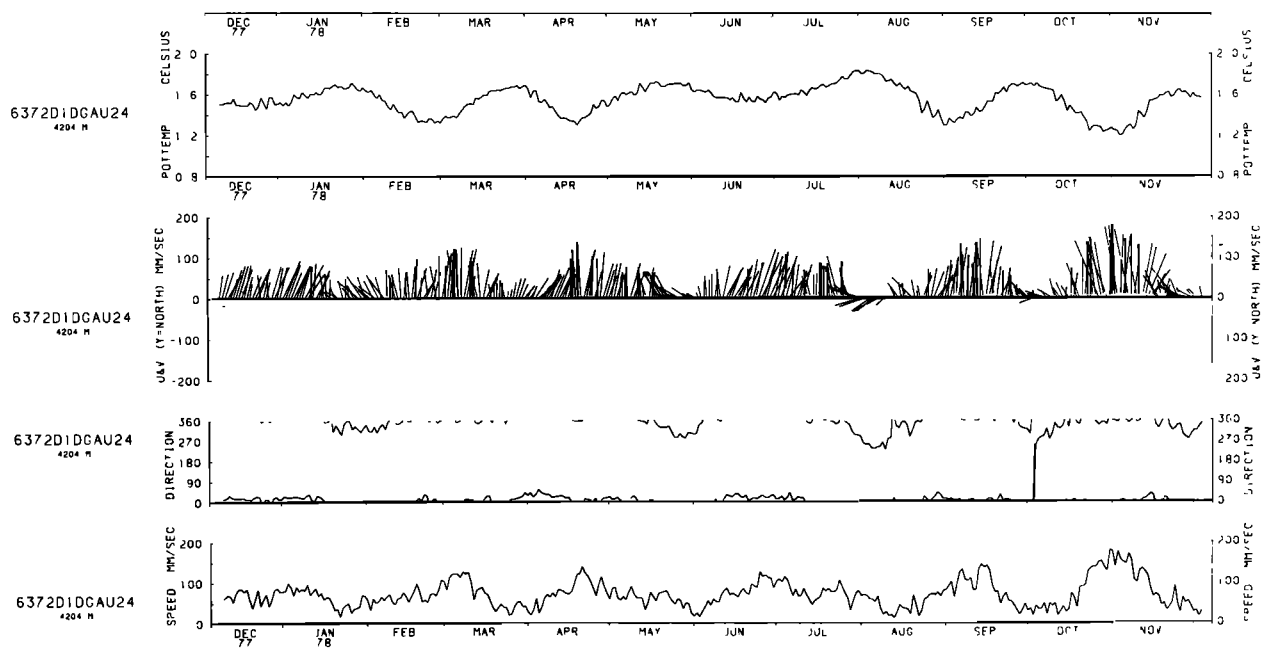

Fig. 8*f*

west mooring and solid squares for the east mooring. Also shown are values of velocity from an exact cubic polynomial solution.

The polynomial for the mooring 636 (west) average velocity field is

$$v_w = 11.987 + 7.9935 \times 10^{-1}h - 6.9537 \times 10^{-3}h^2 + 1.4786 \times 10^{-5}h^3 \quad (2)$$

where h is distance in meters below the top current meter. Numbers from this relation are shown as pluses in Figure 9 and the cubic relation extrapolates smoothly above the mooring, but there is a sharp (and probably nonexistant) change in extrapolated shear below the mooring. The cubic polynomial solution for mooring 637 (east) is

$$v_e = 31.392 + 3.003 \times 10^{-1}h + 1.7909 \times 10^{-3}h^2 - 1.5519 \times 10^{-5}h^3 \quad (3)$$

Numbers from this relation are shown by the cross on Figure 9, and in this case a sharp (and probably nonexistant) change in shear is given by this relation above the mooring, with none below. It was decided to reject the extrapolated values from the above relation and visually extrapolate a smooth curve to the zero velocity axis. These curves are shown as dashed curves.

Because there were only two moorings, information on the horizontal distribution of velocity is limited. To estimate the total northward flux, a width of water must be assigned which that mooring is believed to represent, and equations

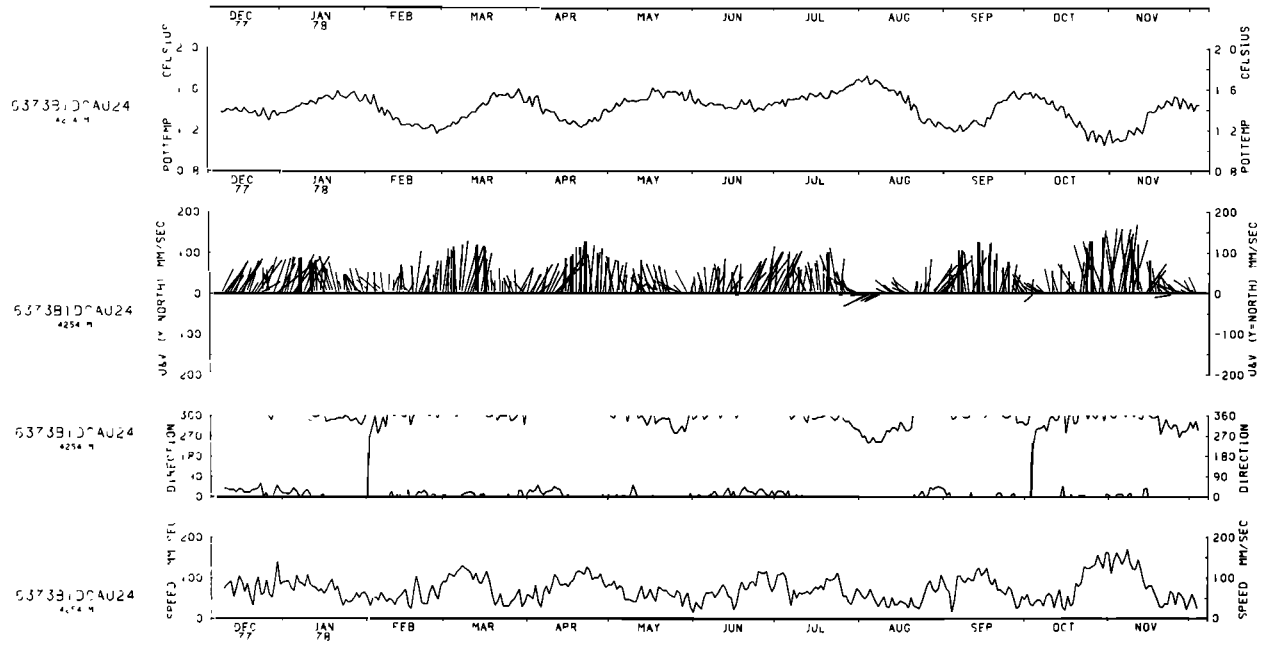

Fig. 8*g*

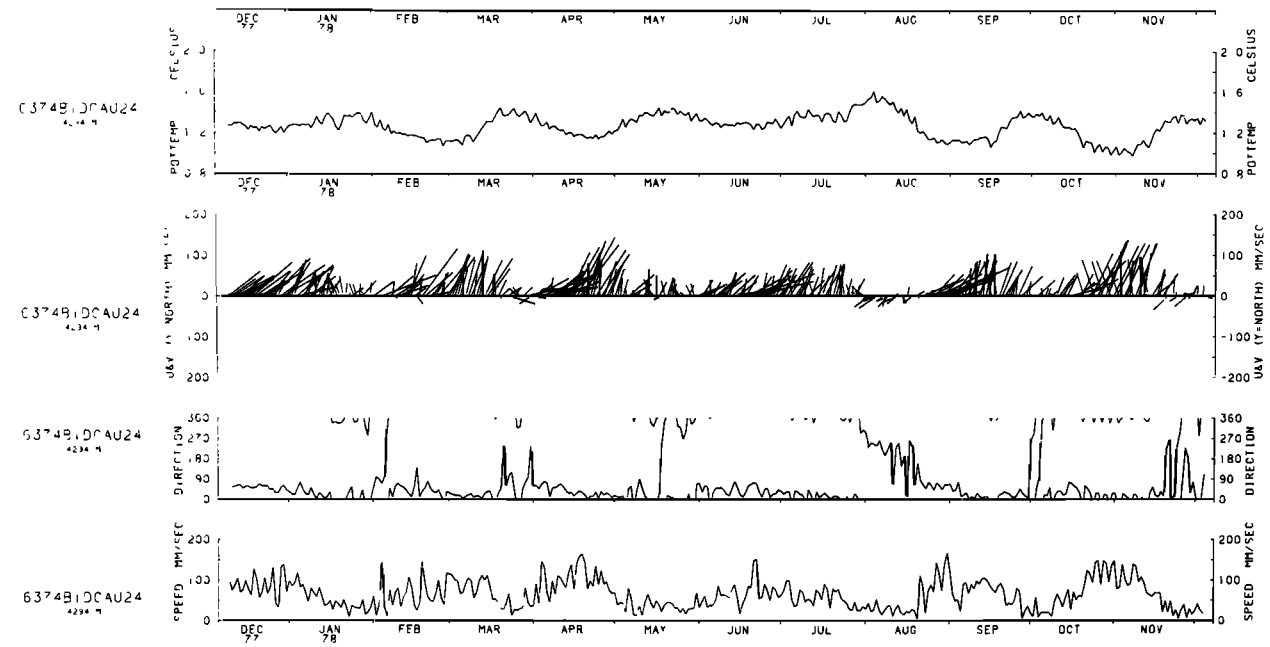

Fig. 8*h*

(2) and (3) must be integrated. This was done between the depths of extrapolated zero velocity, which are a depth of 4239 ($h = -17$) and a depth of 4490 ($h = 234$) for the west mooring. For the east mooring, the polynomial was integrated from a depth of 4104 m ($h = 0$) to a depth of 4340 ($h = 236$), and a small sum was added for the extrapolated flux between depth 4060 to 4104. The integral of velocity times height is thus

$$\int_{-17}^{234} \bar{v}_w dz = 6146 \times 10^{-3} \text{ m}^2/\text{s} \quad (4)$$

and

$$\int_0^{236} \bar{v}_e dz + \left(\frac{64 \times 31.392 \times 10^{-3}}{2}\right) = 12580 \times 10^{-3} \text{ m}^2/\text{s} \quad (5)$$

These numbers were then multiplied by a width of the current. The west mooring was taken to represent the waters

TABLE 1. Some Statistical Features of the Flows

Mooring Depth	$\bar{u}$(mm/s)	$\bar{v}$(mm/s)	$\bar{\theta}$(°C)	θ_c(°C)
West 4256	−2.416	11.987	1.568	−0.096
West 4356	1.707	37.170	1.276	−0.006
West 4406	7.202	25.332	1.146	0.016
West 4446	19.608	14.249	1.055	0.008
East 4104	−2.643	31.392	1.816	−0.035
East 4204	−0.118	63.285	1.554	−0.058
East 4254	0.238	64.315	1.416	−0.045
East 4294	27.814	46.604	1.269	−0.056

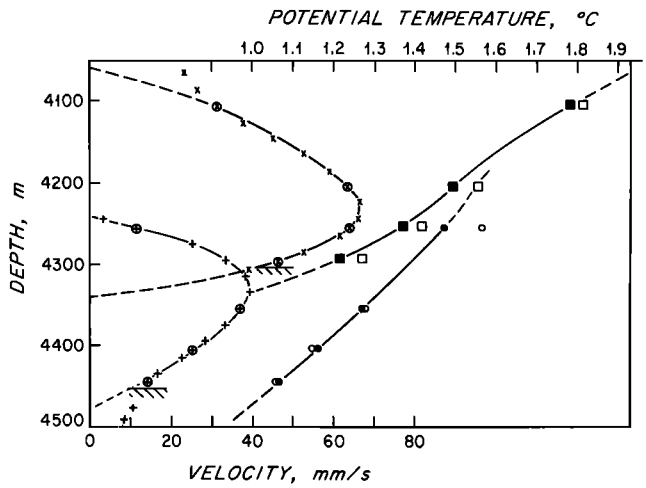

Fig. 9. Mean northward velocity for each current meter as a function of depth (circled pluses for the west mooring and circled crosses for the east mooring). The uncircled pluses and crosses are perfect fit polynomials, the lines are interpolated curves fit by eye, and the dashed lines are extrapolated curves fit by eye as discussed in the text. Temperature is given as open circles for the west mooring and open squares for the east mooring. Temperature plus a 'correction' term (equation (1)) is given as solid circles for the west mooring and solid squares for the east mooring.

between kilometer number 156 and 195 on Figure 4. The 156 kilometer point is the approximate location of the edge of the Ceara Rise, and the 195 kilometer point is the midpoint between the current meters. The value of the width, which the east mooring samples, is more subjective and depends upon the selection of the point where the velocity is believed to become zero to the east. The 240 kilometer point was selected because it is a point where the 1.5° isotherm has leveled off to a considerable extent (see Figure 4). Note that it reached a depth of approximately 4100 m, which is the depth of that isotherm upstream (Figure 6). The width is thus 45 km which may be too large by 10 km or too small by 30 or more. The flux for both alternates will also be calculated as values not to be excluded.

With the above numbers from (4) and (5), volume flux for the west mooring is estimated to be 239.7 × 10^3 m^3/s between the depths 4239 and 4490 meters, which encompasses waters with potential temperature from 0.96°C to 1.50°C. Volume flux for the east mooring is estimated to be 440.3 (minimum), 566.1 (expected), and 943.5 (maximum) × 10^3 m^3/s between the depths of 4060 and 4340 ms, which encompasses waters with potential temperatures between 1.30° and 1.90°C. From the final curves one can also calculate net Eulerian mass flux as a function of potential temperature by measuring the thickness of each water between each 0.1° isotherm and by again assigning a velocity and a width of water which that mooring is believed to represent. The thickness and velocity can be taken directly from Figure 9. The numbers are given in Table 2, and the sums differ from the estimates found by integrating the polynomials by less than 2%. These numbers are our best estimates of volume flux of this water into the North Atlantic based upon the current meter data.

Geostrophic Calculations

To summarize, the east mooring showed low northward velocity in the warm, upper layer (1.9°–1.8°), maximum velocity in the midrange of temperature (1.5°–1.4°), and low velocity again in the cold, deep layer (1.1°–1.0°). The west mooring (636) showed similar results except that the maximum velocity fell in the 1.4°–1.3° layer. In terms of volume transport both moorings indicate that less water flows northward in the warm and cold extremes of Antarctic Bottom Water than is carried in its midrange of temperature. On average, the current meters and temperature recorders indicate that there is a level of no meridional motion near the 1.9° isotherm. The general water mass distribution commends this choice of level, since the 1.9° isotherm is the approximate boundary between the Antarctic Bottom Water and the southward flowing North Atlantic Deep Water.

The first full day of the current meter and temperature

TABLE 2. Estimate of Transport in 0.1°C Intervals Based Upon the Current Meter Data

θ(°C)	v(mm/s)	h(m)	$Q \times 10^{-3}$ m^3/s Minimum (w = 35 km)	$Q \times 10^{-3}$ m^3/s Expected (w = 45 km)	$Q \times 10^{-3}$ m^3/s Maximum (w = 75 km)
			East Mooring		
1.9–1.8	18	29	18.3	23.5	39.2
1.8–1.7	34	28	33.3	42.8	71.4
1.7–1.6	46	35	56.4	72.5	120.8
1.6–1.5	57	42	83.8	107.7	179.6
1.5–1.4	66	41	94.7	121.8	203.0
1.4–1.3	63	32	70.5	90.7	151.2
1.3–1.2	52	24	43.7	56.2	93.6
1.2–1.1	38	20	26.6	34.2	57.0
1.1–1.0	19	19	12.6	16.2	27.1
Total			440.0	565.6	942.9
θ(°C)	v(mm/s)	h(m)		$Q \times 10^{-3}$ m^3/s (w = 39 km)	
			West Mooring		
1.5–1.4	21	51		41.8	
1.4–1.3	38	50		74.1	
1.3–1.2	35	47		64.2	
1.2–1.1	25	46		44.9	
1.1–1.0	12	42		19.7	
Total				244.7	

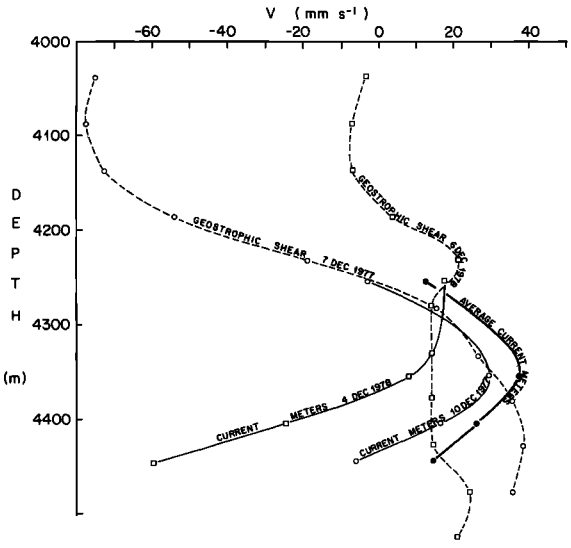

Fig. 10. V (mm s^{-1}) versus depth m. Curves represent current meter data (solid lines) and computed geostrophic shear (dashed lines). For explanation, see text.

record was December 10, 1977, and the last day December 4, 1978. CTD stations were made December 7, 1977, 3 days before the first day of record and hydrographic stations were taken December 6, 1978, 2 days after the last day of record. It is unfortunate that we neglected to make additional CTD and hydrographic stations while the current meters and temperature recorders were in the water because the calculated geostrophic shear is difficult to reconcile with the shear measured by the current meters. The fundamental difference is that the current meters show diminishing northward velocity with depth below the maxima, and calculated geostrophic shear curves, with negligible exceptions, do not.

This is illustrated for the west mooring (635) in Figure 10. Three northward velocity profiles from the current meters are shown for this mooring. The heavy, solid line connects the average northward velocity values at each current meter for the whole 360-day period. A light solid line marked 'current meters, 10 Dec 1977' represents the average northward velocity for the first day of record, and another light solid line marked 'current meters, 4 Dec 1978' is the average for the last day of record. The two dashed lines represent calculated geostrophic shear. The one marked 'geostrophic shear, 7 Dec 1977' was calculated from CTD stations 23 and 24 made on that date, and the other, marked 'geostrophic shear, 6 Dec 1978,' was calculated from hydrographic stations 77 and 78 made on that date; both these pairs of stations bracket the west mooring (Figure 4). The December 7, 1977, geostrophic shear curve has been adjusted to fit the upper part of the current meter curve of December 10, 1977, and the December 6, 1978, geostrophic shear has similarly been adjusted to fit the current meter record of December 4, 1978, as far as is possible.

Allowing for the unfortunate fact that the data are not synoptic, the discrepancies are obvious. A decrease in the northward velocity component took place (below the maximum) in all the three curves based on current meters; it was most marked on the last day of record (December 4, 1978) when the deepest current meter averaged more than 60 mm s^{-1} toward the south. The geostrophic shear curves, on the other hand, show little or no decrease in northward velocity with increasing depth.

Comparison of the Two Estimates

This raises a dilemma: There are clearly two methods of calculating the flux of Antarctic Bottom Water. One method is to take the northward transport from the current meters (Table 2) as representative of the total transport. This method assumes that northward transport is confined to the continental slope near the Ceara Rise and that no considerable flow takes place to the east of the mooring site. This results in a net calculated northward transport of 0.81×10^6 m^3 s^{-1}, more than half of it between isotherms 1.2° and 1.5°. Another approach is to accept the upper level of no meridional motion at 1.9° (as established by the current meters) and to calculate the geostrophic northward flux of water, relative to this isotherm, for the entire section. This assumes that the decreasing velocity with depth observed by the current meters is due to some local topographic effect and also that the reference surface remains constant to the east of the moorings. The geostrophic calculations give a net northward transport of 1.98×10^6 m^3 s^{-1}, more than half of it below the 1.2° isotherm. Of this calculated total, 1.60×10^6 m^3 s^{-1}, or 81%, fell between stations 22–24 and 24–19. These stations bracketed the moorings near the Ceara Rise (Figure 4), so regardless of which method is more correct, the major northward flux was near the Ceara Rise where we placed the current meters. Note that topography capable of constricting the current lies north and south of the 4° section. On the left (Figure 2) is a small ridge approximately 10 km north of the 4°N section. This extends eastward almost as far as the location of the west mooring and may be blocking the waters west of this mooring. On the right are ridges both north and south of the section. Their 4250 m contour extends from the Mid-Atlantic ridge westward to CTD station 17. Whether this ridge extends up into the important region between 4000 and 4250 m is unknown, but it certainly is a possible blockage to waters east of station 17. In any case, both the existence of ridges near the 4°N section, and the geostrophic calculation, are consistent with the widths used.

Another possible source of the disagreement concerns the mean velocity of the bottom current meters, which is smaller than velocity above. The geostrophic estimates gave significantly higher fluxes for water at the bottom. It is not known whether the disagreement lies in errors of the current meter interpretation or the geostrophic calculation. Both have weaknesses. Clearly a geostrophic calculation could be considered to be suspect for a number of reasons: We are, of course, very close to the equator, where the geostrophic approximation is less reliable. The passageways may not all be connected to each other below the depth of the peaks of the topography so that there may be closed basins. Or perhaps there is enough friction near the bottom to counteract geostrophy. Needless to say, if we had taken one of the extrapolated zero crossings other than the 1.9° isotherm of the current meter data as a level (or isotherm) of no motion, we would have obtained widely different and, in our opinion, absurd results. Likewise, the data for the bottom current meters might be deceptive for a number of reasons: the meter may be behind some local obstacle, or there may be a local boundary layer on the seamount which is absent between seamounts. In this latter regard, the fact that both

bottom currents veer to the right is possibly not accidental. Is the veering a local topographic effect [*Bryden*, 1980]?

Which of the calculations are more correct cannot be resolved here. The low mean flows of the bottom current meters are due to the veering of the current and the reversals during slack periods, neither process seems to be closely coupled to frictional effects. It seems best to regard the current meter estimates as lower bounds and the geostrophic calculations as upper bounds with close agreement for waters between 1.2° and 1.9°C and strong disagreement for waters colder than 1.2°C. Since this dilemma is unresolved, we have calculated the various water and heat fluxes and the residence times using both methods.

3. Calculation of Residence Times, Water, and Heat Fluxes in Antarctic Bottom Water in the Western North Atlantic

By the methods described above, we have estimated the volume flux of Antarctic Bottom Water at 4°N to be 0.81×10^6 m^3 s^{-1} according to current meter data and 1.98×10^6 m^3 s^{-1} according to geostrophic calculations. Here we discuss the fate of this water as it flows into the western basin of the North Atlantic. Since the current meters indicated that, on average, all water colder than 1.9° was flowing north, we define all water below this isotherm as Antarctic Bottom Water. By this definition, there are 7.2×10^6 km^3 of Antarctic Bottom Water in the western North Atlantic, according to *Wright and Worthington* [1970]. These authors calculated the volumes of deep water that lie between each 0.1° temperature interval, and it was for this reason that we have calculated the northward flux at 4°N by the same intervals, so that residence times and mixing rates can be calculated for each 0.1° layer. We have also calculated the upward advection of water and salt and the downward diffusion of heat and salt across each of these surfaces. From these we have estimated the vertical mixing coefficients for heat and salt. The validity of these residence times and mixing coefficients depends on two assumptions: first, that the volume of Antarctic Bottom Water in each 0.1° layer has continued to remain constant in recent times and, second, that we have calculated the northward flux of water at 4°N correctly.

Regarding the first assumption, we have found no evidence that the volume of Antarctic Bottom Water is changing in any layer. We have compared temperature/depth curves from the *Meteor* Expedition of 1925–1927, from the International Geophysical Year of 1957–1958, and from our own CTD and hydrographic stations in 1977 and 1978 without finding any systematic difference. While we cannot entirely rule out small changes in the volume of Antarctic Bottom Water over the years, the assumption of a steady state seems most reasonable. If we assume a steady state, it follows that there must be upward advection of water across each isotherm, balanced by a downward (cross isotherm) diffusion of heat [*Stommel*, 1958]. Regarding the second assumption, there is more doubt; the northward flux of water at 4°N can be calculated by two methods (at least) which have been fully described and which give widely different results.

While the calculation of the northward flux of Antarctic Bottom Water and its residence time in the North Atlantic is perfectly simple, the calculation of heat fluxes is slightly more complicated since, among other things, the geothermal heat flux must be taken into account. We have summarized these calculations in Table 3, which needs some explanation.

The top half of this table represents the fluxes, etc., obtained by using the current meter velocities as described in Table 2. The bottom half is obtained by assuming a reference surface at 1.9° throughout the CTD section at 4°N (Figure 4). The method used to divide the geostrophic transports into the different layers has been described by *Worthington* [1976]. In this table all values on a line refer to an isothermal surface; all values in a box (on the half line) refer to a layer between two isothermal surfaces. Thus, column 1 (on lines) lists the temperature surfaces that bound each 0.1° layer. Column 2 (in boxes) is the mean temperature of each layer. Column 3 gives the volume transport into each layer at 4°N. Column 4 (on lines) gives the cumulation of these transports from the bottom up; since each layer is assumed to contain a fixed volume of water, and the ocean bottom is assumed to be impervious, these cumulations must cross each successive isothermal surface. Column 5 represents the area of each isothermal surface in the western North Atlantic north of 4°. This was determined by counting the number of 1° squares (latitude × longitude) on each 1° interval of latitude embraced by each isothermal surface, and multiplying by the area of each square. For this we used the large-scale worksheets prepared by Worthington and Wright for their 1970 atlas. Column 6 is the area of the upper isotherm less the area of the lower isotherm that bounds each layer.

Column 7 is the rate of geothermal heat flow expressed in 10^{-6} cal cm^{-2} s^{-1}. For this we used charts provided by J. G. Sclater (personal communication, 1980) giving the age of the American Basin of the North Atlantic. We read off the average age for that part of each layer which was exposed to the bottom. These ages were converted to heat flow by a correlation in *Sclater et al.* [1980, Table 1]. These averages did not differ significantly from the individual measurements of heat flow, which were also printed on the charts. Column 8 gives the net amount of heat entering each layer through the ocean bottom (column 6 × column 7). Column 9 gives the flux of heat into each layer at 4°N (column 2 × column 3). Column 10 gives the total heat crossing each isothermal surface from below (column 1 × column 4). Column 11 gives the total heat advected into each layer (columns 8, 9 and 10): For example, the layer 1.8° to 1.9° receives 21×10^9 cal s^{-1} from geothermal heat flow (column 8), 43×10^9 cal s^{-1} from the influx at 4°N (column 9), and 1416×10^9 cal s^{-1} in heat advected upward across the 1.8° surface (column 10); these add up to 1480×10^9 cal s^{-1} (column 11). Since a total of 1540×10^9 cal s^{-1} leaves the layer by upward advection, 223×10^9 cal s^{-1} leaves the layer by downward diffusion, and only 1480×10^9 cal s^{-1} enters the layer by advection, the difference, 283×1^9 cal s^{-1} must enter the layer by downward diffusion of heat. Column 12 gives this downward diffusion of heat across each isothermal surface. Column 13 gives the rate of this downward diffusion of heat per unit area expressed in 10^{-6} cal cm^{-2} s^{-1} (column 12 divided by the area of each isotherm given in column 5).

Column 14 is upward advection velocity (10^{-5} cm s^{-1}) of water across each isothermal surface (column 4 divided by column 5); column 15 is the same quantity expressed in meters per year. Column 16 is the volume of water in the

TABLE 3. Estimate of Volume Transport, Heat Flux, and Residence Time of Water Colder Than 1.9° in the North Atlantic

Potential Temperature, (θ)	Mean θ, each layer, °C	N. volume flux at 4°N into each layer, 10^6 m^3 s^{-1}	Volume advected across each isotherm, 10^6 m^3 s^{-1}	Area of each isotherm 10^{13} cm^2	Area between each isotherm 10^{13} cm^2	Geothermal heat flux 10^{-6} cal cm^{-2} s^{-1}	Total geothermal heat flux into each layer (6x7), 10^9 cal s^{-1}	N. heat flux at 4°N (2x3), 10^9 cal s^{-1}	Total heat crossing each isotherm (1x4) 10^9 cal s^{-1}	Total heat flux into each layer 10^9 cal s^{-1} (8+9+10)	Downward diffusion of heat across each isotherm 10^9 cal s^{-1}	Downward diffusion heat/unit area (12÷5), 10^{-6} cal cm^{-2} s^{-1}	Upward advection of water (4÷5), 10^{-5} cm s^{-1}	Upward advection of water (14x31.557) 10^{-6}, m y^{-1}	Volume (N of 4°N) of each layer, 10^3 km^3	Volume transport into each layer (4x31.56), 10^3 km^3 y^{-1}	Residence time in each layer (16÷17), y
1	2	3	4	5	6	7	8	9	10	11	12	13	14	15	16	17	18
(a) Current Meter Transport																	
1.9			.8103	8205					1540		283	3.45	1.0	3.1			
1.8	1.85	.0235	.7868	6504	1701	1.25	21	43	1416	1480	223	3.43	1.2	3.8	2773	25.6	108
1.7	1.75	.0428	.7440	4784	1720	1.27	22	75	1265	1362	169	3.53	1.6	4.9	1454	24.8	59
1.6	1.65	.0725	.6715	3500	1284	1.33	17	120	1074	1211	115	3.29	1.9	6.1	1002	23.5	43
1.5	1.55	.1077	.5638	2382	1118	1.29	14	167	846	1027	68	2.85	2.4	7.5	938	21.2	44
1.4	1.45	.1636	.4002	1296	1086	1.52	17	237	560	814	36	2.78	3.1	9.7	482	17.8	27
1.3	1.35	.1648	.2354	509	787	1.50	12	222	306	540	16	3.14	4.6	14.6	281	12.6	22
1.2	1.25	.1204	.1150	191	318	1.86	6	151	138	295	5	2.62	6.0	19.0	49	7.4	7
1.1	1.15	.0791	.0359	55	136	1.85	3	91	39.5	133	0.8	1.45	6.5	20.6	9	3.6	2.5
1.0	1.05	.0359		0	55	1.85	1.0	37.7		38.7					2.2	1.1	1.9
(b) Geostrophic Transport Referenced to 1.9°																	
1.9			1.982	8205					3766		1142	13.92	2.4	7.6			
1.8	1.85	.013	1.969	6504	1701	1.25	21	24	3544	3589	965	14.84	3.0	9.6	2773	62.6	44
1.7	1.75	.085	1.884	4784	1720	1.27	22	149	3203	3374	795	16.62	3.9	12.4	1454	62.1	23
1.6	1.65	.125	1.759	3500	1284	1.33	17	206	2814	3037	629	17.97	5.0	15.9	1002	59.5	17
1.5	1.55	.139	1.620	2382	1118	1.29	14	215	2430	2659	474	19.90	6.8	21.5	938	55.5	17
1.4	1.45	.230	1.390	1296	1086	1.52	17	334	1946	2297	341	26.31	10.7	33.8	482	51.1	9
1.3	1.35	.130	1.260	509	787	1.50	12	176	1638	1826	221	43.42	24.8	78.1	281	43.9	6
1.2	1.25	.153	1.107	191	318	1.86	6	191	1328	1525	108	56.54	58.0	182.9	49	39.8	1.2
1.1	1.15	.531	.576	55	136	1.85	3	611	634	1248	28	50.91	104.7	330.5	9	34.9	0.3
1.0	1.05	.576		0	55	1.85	1.0	605	0	606					2.2	18.2	0.1

western North Atlantic in each layer north of 4°N. This was obtained by subtracting the volume between 0° and 4°N from the values in *Wright and Worthington* [1970] using their worksheets. Column 17 is the volume transport into each layer; the same values as column 4, but expressed in 10^3 km^3 y^{-1}. Column 18 is the mean residence time of water in each 1.0° layer.

All the northward volume transport of Antarctic Bottom Water takes place below the 1.9° isotherm, but, as we have mentioned, the two methods of computing this transport give quite different quantities. The greatest difference is found in the coldest water (<1.2°). The current meter data give a transport of 0.115×10^6 m^3 s^{-1} below 1.2°, and the geostrophic calculations referenced to 1.9° give 1.107×10^6 m^3 s^{-1}, roughly 10 times as much. While geostrophy is widely accepted as holy writ [see *Clarke et al.*, 1980, p. 48], there are reasons for supposing that the current meters, in this particular case, give a more accurate estimate of the northward flux of Antarctic Bottom Water. We will give some of these reasons below; however, all fluxes, mixing rates, etc., are calculated by both methods.

The most compelling reason in favor of using the current meter data is that direct measurement is preferable to calculation whenever possible. The deepest current meters were in the coldest Antarctic Bottom Water at 4°N and while there was a good deal of fluctuation, they state, unanimously, that the cold water had little net northward movement. The average measured northward velocity for water between 1.0° and 1.1° was 20.8 mm s^{-1}, for a total of 403 current meter days. For 43 current meter days the temperature dropped below 1.0°, and the mean meridional velocity during this period was 2 mm s^{-1} to the south (for practical purposes zero).

There are 2.2×10^3 km^3 of water between 1.0° and 1.1° in the North Atlantic north of 4° (Table 3). If the geostrophic method is followed, the mean residence time of this water must be 0.1 years. The area of the 1.1° isotherm is 55×10^{13} cm^2. A flux of 0.576×10^6 m^3 s^{-1} requires an upward movement of 330.5 m y^{-1} across this surface (Table 3). While neither this residence time nor this upward velocity can be rejected out of hand, the values obtained from the current meter data—1.9 years and 20.6 m year (Table 3)—seem far more 'reasonable.' Similarly, the geostrophic transports require a much larger downward diffusion of heat across each isothermal surface than do the current meter transports, especially in the colder layers; downward diffu-

sion calculated from the current meter data range between 1.45 and 3.45 × 10^{-6} cal cm^{-2} s^{-1} with a general, but, small decrease toward the colder layers. In contrast, downward diffusion from geostrophic calculations increases rapidly with decreasing temperature from 13.92 × 10^{-6} cal cm^{-2} s^{-1} across the 1.9° surface to 50.91 × 10^{-6} cal cm^{-2} s^{-1} across the 1.1° surface. The implied eddy diffusivities (Table 4) from the geostrophic calculations range up to 7.73 cm^2 s^{-1}, a value more than 10 times that usually discussed in connection with the deep ocean. Another problem with the numbers associated with the geostrophic mass flux concerns the large bottom velocities that are implied in the North Atlantic. The 0.1-year residence time that is calculated for the 1.0°–1.1°C water implies an average northward velocity of 12 cm s^{-1} in order to fill the volume, while the water immediately above would have a velocity of 4.6 cm s^{-1}. Since both isotherms have descended approximately 200 m between the 4°N section (Figure 4) and the section further north (Figure 3), and there is even evidence for slower geostrophic flow of the 1.0°–1.1° water in this figure, vertical shear is unlikely.

In addition, the 12 cm s^{-1} velocity would produce a tilt of the 1.1°C isotherm in Figure 3 of at least 14 m/km which is not there. With an Ekman number of approximately 0.009 (using viscosity that is equal to the diffusivity of 2.8 cm^2 s^{-1}, a depth of 40 m and Coriolis parameter of 2 × 10^{-5}), it is not possible to attribute the lack of tilt to turbulent drag.

In effect, of course, what all these comparative calculations reflect is that there is very little cold (<1.2°) Antarctic Bottom Water in the North Atlantic and it occupies a minute area of that ocean [*Worthington and Wright*, 1970, plates 4, 5, 6, and 7]. Geostrophy relative to the 1.9° surface requires a very large northward flux of this cold water and this results (in our opinion) in unreasonable properties such as short residence times, unreasonably large velocities, and unreasonable dynamics. These, in turn, require excessive downward diffusion of heat.

Mixing Rates of Antarctic Bottom Water

The calculation of vertical mixing rates is complicated slightly by the fact that these rates depend on vertical temperature gradients. These gradients are relatively strong near 4°N, but become progressively weaker with increasing latitude north. One could, of course, normalize the mixing rate by assuming a more rapid upward advection of water near 4°S and progressively slower upward advection further north. We feel that this is not justified because nothing is known about the actual velocity of upward advection. Our own estimates of upward velocity are higher than most, particularly in the colder water. *Veronis* [1977] has reviewed a number of estimates of upward velocity; and none of these exceed 7 m y^{-1}. Veronis' interest was in ocean-wide models rather than localized experiments like ours but, nevertheless, our estimate of 20.6 m y^{-1}, across the 1.1° isotherm (Table 3 (top)) based on our current measurements seems on the high side, and the value of 330.5 m y^{-1} (Table 3 (bottom)) for the same isotherm based on geostrophic calculations is unheard of.

Accordingly, we have calculated the vertical mixing coefficient (Table 4) for the different zones of north latitude. The downward diffusion of heat in the second column of this table is taken from Table 3 (column 13) and is assumed to be constant across the whole area of each isothermal surface.

The vertical temperature gradients (dT/dz) given in Table 4 are the average gradients, within each latitude zone, from all the hydrographic stations in the western North Atlantic used in *Worthington and Wright*'s [1970] atlas, plus those from our own CTD and hydrographic stations made during this investigation. The gradients vary from 30.3 × 10^{-6} °C cm^{-1} at the 1.5° isotherm in the 4°–10° zone to 1.8 × 10^{-6} °C cm^{-1} at the 1.5° isotherm in the 35°–40° and the 40°–43° zone. (Stations in the Labrador Basin as defined by *Wright and Worthington* [1970], are omitted since this basin contains no Antarctic Bottom Water.)

The calculated mixing rates, based on current meter transport (Table 4 (top)), vary from 0.094 cm^2 s^{-1} at the 1.5° isotherm in the 4°–10° zone to 1.917 cm^2 s^{-1} at the 1.9° isotherm in the 35°–40° and 40°–43° zones. The average mixing coefficient ($\bar{K}$) at each isotherm is given in the last column. $\langle\bar{K}\rangle$, the average of all 34 mixing coefficients, is given at the foot of the column; this value 0.741 cm^2 s^{-1} is the best estimate we can make for the average mixing rate based on current meter transport. The mixing coefficients based on geostrophic calculations relative to 1.9° (Table 2 (bottom)) are generally higher since the downward diffusion of heat required by these calculations is higher.

We have also calculated the downward diffusion of salt both from the current meter transport (Table 5 (top)) and the geostrophic transport relative to 1.9° (Table 5 (bottom)). The method of constructing this table closely follows Table 3 and needs no detailed explanation. It should be mentioned, however, that the values of salinity at each isotherm in this table were taken from the θ/S plot of all the stations made in this investigation which included a section from 8°S to 28°N. They are slightly fresher than the statistical values of *Worthington and Metcalf* [1961].

The downward diffusion of salt based on current meter transport shown in column 11 (Table 5 (top)), varies between 3.64 × 10^{-10} g cm^{-2} s^{-1} at the 1.1° isotherm and 5.96 × 10^{-10} g cm^{-2} s^{-1} at the 1.7° isotherm. As one would expect, the variation in downward diffusion of salt is far greater for the geostrophic transport (Table 5 (bottom)), varying from 17.79 × 10^{-10} g cm^{-2} s^{-1} at the 1.9° isotherm to 68.06 × 10^{-10} g cm^{-2} s^{-1} at the 1.2° isotherm.

The salt mixing rates (Table 6) are, again, computed in the same manner as was done for heat. The mean salt diffusion coefficient for current meter transport was 1.063 cm^2 s^{-1} compared with 0.741 cm^2 s^{-1} for heat. The salt mixing rates for geostrophic transport are larger because the required downward diffusion of salt is larger.

A further consideration is that the real mixing across the isothermal surfaces of Antarctic Bottom Water may be horizontal rather than vertical. It can be seen from Figure 1, and from *Worthington and Wright* [1970, even numbered plates 4–20] that the 1.1° to 1.9° temperature surfaces slope downward from the sill near 4°N into the North American Basin. We have roughly estimated these slopes, and from them we have calculated horizontal (across constant potential temperature, which has a small along-isopycnal component) diffusion rates. These are given by the ratio of the (true) vertical to the horizontal gradients. Since the horizontal flux is a factor of l/h larger than the vertical flux (per unit area), and the horizontal gradient is a factor of h/l smaller than the vertical gradient, the equivalent horizontal diffusivity is a factor of l^2/h^2 (= $1/\tan^2\theta$) larger than the vertical diffusivity.

The horizontal diffusivity (K_h) for each isothermal surface

TABLE 4. Estimate of

North Latitude		4°–10°		10°–15°		15°–20°		20°–25°	
°C Potential Temperature	Q, Downward Diffusion of Heat 10^{-6} cal cm^{-2} s^{-1}	$\frac{dT}{dz}10^{-6}$ °C cm^{-1}	K, Mixing Coefficient, cm^2 s^{-1}	$\frac{dT}{dz}10^{-6}$ °C cm^{-1}	K, Mixing Coefficient, cm^2 s^{-1}	$\frac{dT}{dz}10^{-6}$ °C cm^{-1}	K, Mixing Coefficient, cm^2 s^{-1}	$\frac{dT}{dz}10^{-6}$ °C cm^{-1}	K, Mixing Coefficient, cm^2 s^{-1}
									Current Meter Transport
1.9	3.45	6.7	0.515	4.8	0.719	4.2	0.821	3.5	0.986
1.8	3.43	8.6	0.399	5.8	0.591	4.4	0.780	4.0	0.858
1.7	3.53	15.2	0.232	9.3	0.380	5.1	0.692	5.0	0.706
1.6	3.29	21.3	0.154	10.2	0.323	5.4	0.609	3.2	1.028
1.5	2.85	30.3	0.094	8.6	0.331	3.6	0.792		
1.4	2.78	26.3	0.106	13.9	0.200				
1.3	3.14	14.9	0.211						
1.2	2.62	14.1	0.186						
1.1	1.45	15.3	0.095						
$\langle\bar{K}\rangle$									
									Geostrophic Transport Referenced to 1.9°
1.9	13.92	6.7	2.078	4.8	2.900	4.2	3.314	3.5	3.977
1.8	14.84	8.6	1.726	5.8	2.559	4.4	3.373	4.0	3.710
1.7	16.62	15.2	1.093	9.3	1.787	5.1	3.259	5.0	3.324
1.6	17.97	21.3	0.844	10.2	1.762	5.4	3.328	3.2	5.616
1.5	19.90	30.3	0.657	8.6	2.314	3.6	5.528		
1.4	26.31	26.3	1.000	13.9	1.893				
1.3	43.42	14.9	2.914						
1.2	56.54	14.1	4.010						
1.1	50.91	15.3	3.327						
$\langle\bar{K}\rangle$									

TABLE 5. Estimate of Salt Flux for Waters Colder Than 1.9° in the North Atlantic

Potential Temperature °C	Salinity, °/₀₀, at each isotherm	Mean Salinity, °/₀₀, each layer	Volume, 10^6 m^3 s^{-1}, advected into each layer at 4°N	Volume, 10^6 m^3 s^{-1}, advected across each isotherm	Salt, 10^9 g s^{-1}, advected into each layer at 4°N	Salt, 10^9 g s^{-1}, advected upward across each isotherm	Total salt, 10^9 g s^{-1}, advected into each layer	Downward diffusion of salt, 10^9 g s^{-1}, across each isotherm	Area of each isotherm, 10^{13} cm^2
1	2	3	4	5	6	7	8	9	10
				(a) Current Meter Transport					
1.9	34.892			.8103		28.2730		.0465	8205
		34.886	.0235		.8198		28.2642		
1.8	34.881			.7868		27.4444		.0377	6504
		34.875	.0428		1.4927		27.4352		
1.7	34.869			.7440		25.9425		.0285	4784
		34.862	.0725		2.5275		25.9333		
1.6	34.856			.6715		23.4058		.0193	3500
		34.850	.1077		3.7533		23.3983		
1.5	34.844			.5638		19.6450		.0118	2382
		34.838	.1636		5.6995		19.6397		
1.4	34.833			.4002		13.9402		.0065	1296
		34.827	.1648		5.7395		13.9366		
1.3	34.822			.2354		8.1971		.0029	509
		34.817	.1204		4.1920		8.1953		
1.2	34.811			.1150		4.0033		.0011	191
		34.805	.0791		2.7531		4.0024		
1.1	34.799			.0359		1.2493		.0002	55
		34.794	.0359		1.2491		1.2491		
1.0	34.787								0
				(b) Geostrophic Transport Referenced to 1.9°					
1.9	34.892			1.982		69.1559		.1460	8205
		34.886	.013		.4535		69.1342		
1.8	34.881			1.969		68.6807		.1243	6504
		34.875	.085		2.9644		68.6576		
1.7	34.869			1.884		65.6932		.1012	4784
		34.862	.125		4.3578		65.6695		
1.6	34.856			1.759		61.3117		.0775	3500
		34.850	.139		4.8442		61.2915		
1.5	34.844			1.620		56.4473		.0573	2382
		34.838	.230		8.0127		56.4306		
1.4	34.833			1.390		48.4179		.0406	1296
		34.827	.130		4.5275		48.4032		
1.3	34.822			1.260		43.8757		.0259	509
		34.817	.153		5.3270		43.8628		
1.2	34.811			1.107		38.5358		.0130	191
		34.805	.531		18.4815		38.5257		
1.1	34.799			.576		20.0442		.0029	55
		34.794	.576		20.0413		20.0413		
1.0	34.787					0			0

Temperature Mixing Coefficient

25°–30°		30°–35°		35°–40°		40°–43°		
$\frac{dT}{dz}\ 10^{-6}$ °C cm^{-1}	K, Mixing Coefficient, cm^2 s^{-1}	$\frac{dT}{dz}\ 10^{-6}$ °C cm^{-1}	K, Mixing Coefficient, cm^2 s^{-1}	$\frac{dT}{dz}\ 10^{-6}$ °C cm^{-1}	K, Mixing Coefficient, cm^2 s^{-1}	$\frac{dT}{dz}\ 10^{-6}$ °C cm^{-1}	K, Mixing Coefficient, cm^2 s^{-1}	$\bar{K}$
3.3	1.045	2.8	1.232	1.8	1.917	1.8	19.17	1.144
3.2	1.072	3.3	1.039	2.3	1.491			0.890
3.1	1.139	3.4	1.038					0.698
2.2	1.495							0.722
								0.406
								0.153
								0.211
								0.186
								0.095
								0.741
3.3	4.218	2.8	4.971	1.8	7.733	1.8	7.733	4.616
3.2	4.638	3.3	4.497	2.3	6.452			3.851
3.1	5.361	3.4	4.888					3.285
2.2	8.168							3.944
								2.833
								1.447
								2.914
								4.010
								3.327
								3.675

(1.9°–1.1°) is given in Table 7. This table has certain defects in that it takes into account only the mean slopes of the isotherms (disregarding bumps) and, of course, where the downslope approaches 0° the calculated diffusivity approaches infinity.

Discussion

Since the θ/S relationship was nearly linear with little scatter (see Table 5, columns 1 and 2) temperature and salinity are proportional in each layer. Therefore, the vertical mixing rates for heat and salt should be identical. The GEOSECS data indicate that other tracers are likewise linearly related to temperature. In fact, if one performs the calculations with the geothermal heat flux removed the mixing rates for salt, are the same as the rates for heat.

We do not question the accuracy of the geothermal heat fluxes obtained from *Sclater et al.* [1980], and we believe that our average vertical diffusion coefficient 0.741 cm^2 s^{-1} for the current meters is reasonable, nor can the difference between heat and salt mixing rates be dependent on geothermal heat flux. The discrepancy may lie with double-diffusive transport. However, the difference between salt and temperature diffusivities is larger than that believed to occur due to double diffusion. Perhaps the discrepancy lies in more subtle effects to do with the equation of state or along-isopycnal mixing.

It is also possible that the θ/S relationship does, in fact, vary as a function of time and space. There is some variation of salinity at potential temperature isotherms (Worthington and Wright) which is consistent with geothermal heating. Salinity is consistently lower near the edges of the tongues protruding into the North Atlantic for temperatures colder than 1.6. This is consistent with cold low salinity water being heated in contact with the bottom, so that its potential temperature is slightly increased. There is even a local salinity minimum at 22°N in the 1.6° isotherm which correlates with a topographic bump.

With respect to temporal variability, we have noted above that our values of salinity are slightly lower than those reported by Worthington and Metcalf (1961). The differences at and above 1.7° (0.008 ‰ to 0.010 ‰) are in part due to geography. Since our section (Figure 1) stopped at 28°N, 55°W, we did not observe the slightly more saline waters (at 1.7°–1.9°) that lie to the north and west of our observations according to *Worthington and Wright* [1970, plates 17, 19, and 20] and are included in *Worthington and Metcalf*'s [1961] θ/S curve. The differences below 1.6° are harder to explain. They average 0.005 ‰ fresher than *Worthington and Metcalf*'s [1961] values but are in the same geographical area [see *Worthington and Wright,* 1970, odd numbered plates 3–13]. They could be due to a real freshening of Antarctic Bottom Water, but they could also be due, at least in part, to differences in individual batches of standard water of the kind described by *Mantyla* [1980]. However, we have not been able to unearth the batch numbers used by Woods Hole observers during the International Geophysical Year.

We had hoped, by measuring the flux of Antarctic Bottom Water into the North Atlantic accurately, to determine mixing rates for heat and salt that would be more widely useful in the oceans. This we clearly have not done to scientifically acceptable standards for the water between 1.0° and 1.2°C. The wide difference between mixing rates (and residence times, vertical velocities, etc.) obtained from using current meter data (which we tend to favor) and those obtained by the geostrophic calculations (which is traditionally accepted) make it plain that our data set was not definitive. It appears to be unlikely that the true numbers will be less than the current meter numbers or more than the geostrophic numbers; hence it seems safe to conclude that the correct numbers have been bracketed.

4. Remarks on the Dynamics in the Control Region

In recent years there has been considerable effort to develop an understanding of the effect of rotation in critical control problems in hydrodynamics. An important objective

TABLE 6. Estimate of

North Latitude		4°–10°		10°–15°		15°–20°		20°–25°	
°C Potential Temperature	Q_s, Downward Diffusion of Heat 10^{-10} g cm^2 s^{-1}	$\frac{dS}{dz}$ 10^{-10} g cm^{-4}	K_s cm^2 s^{-1}	$\frac{dS}{dz}$ 10^{-10} g cm^{-4}	K_s cm^2 s^{-1}	$\frac{dS}{dz}$ 10^{-10} g cm^{-4}	K_s cm^2 s^{-1}	$\frac{dS}{dz}$ 10^{-10} g cm^{-4}	K_s cm^2 s^{-1}
								Current Meter Transport	
1.9	5.67	7.38	0.768	5.26	1.078	4.58	1.238	3.89	1.458
1.8	5.80	10.34	0.561	6.94	0.836	5.29	1.096	4.86	1.193
1.7	5.96	19.70	0.303	12.04	0.495	6.67	0.894	6.47	0.921
1.6	5.51	25.53	0.216	12.24	0.450	6.45	0.854	3.83	1.439
1.5	4.95	33.33	0.149	9.48	0.522	3.97	1.247		
1.4	5.02	28.95	0.173	15.28	0.329				
1.3	5.70	16.42	0.347						
1.2	5.76	16.90	0.341						
1.1	3.64	18.46	0.197						
$\langle\bar{K}\rangle$									
								Geostrophic Transport Referenced to 1.9°	
1.9	17.79	7.38	2.411	5.26	3.382	4.58	3.884	3.89	4.573
1.8	19.11	10.34	1.848	6.94	2.754	5.29	3.612	4.86	3.932
1.7	21.15	19.70	1.074	12.04	1.757	6.67	3.171	6.47	3.269
1.6	22.14	25.53	0.867	12.24	1.809	6.45	3.433	3.83	5.781
1.5	24.06	33.33	0.722	9.48	2.538	3.97	6.060		
1.4	31.33	28.95	1.082	15.28	2.050				
1.3	50.88	16.42	3.099						
1.2	68.06	16.90	4.027						
1.1	52.73	18.46	2.856						
$\langle\bar{K}\rangle$									

is ultimately to be able to determine the fluxes through controlling passage ways like the Ceara Abyssal Plain as a function of the density distributions upstream and downstream of the passage. Present theoretical and laboratory studies concern two-layer, steady flows in geometries such that friction is negligible. There are many instances where the formulae from these models predict fluxes which are approximately the same magnitude as the measured fluxes in the ocean [*Whitehead,* 1980; *Hogg et al.,* 1981]. Such formulae can never give more than approximate agreement because of the large differences between the simple two-layer system and the complicated ocean.

It is, however, useful to calculate whether the data set shows that certain properties are conserved in order to assess the appropriateness of the starting assumptions used in the theories. There are, in fact, two time scales at approximately 3 and 60 days (Figure 11). *Eriksen* [1982] has discussed the possibility that the 3-day oscillation comes

TABLE 7. Estimated Vertical or Horizontal Diffusivities

Potential Temperature, °C	K_v cm^2 s^{-1} (from Table 4)	$h \div 1 = \tan\theta$	$K_{h'}$ 10^6 cm^2 s^{-1} = $K_v \div \tan^2\theta$
	Current Meter Transport		
1.9	1.144	0.00011	94.55
1.8	0.890	0.00026	13.17
1.7	0.698	0.00030	7.76
1.6	0.722	0.00035	5.89
1.5	0.406	0.00051	1.56
1.4	0.153	0.00059	0.44
1.3	0.211	0.00072	0.41
1.2	0.186	0.00084	0.26
1.1	0.095	0.00096	0.10
	Geostrophic Transport Referenced to 1.9°		
1.9	4.616	0.00011	381.49
1.8	3.851	0.00026	56.97
1.7	3.285	0.00030	36.50
1.6	3.944	0.00035	32.20
1.5	2.833	0.00051	10.89
1.4	1.447	0.00059	4.16
1.3	2.914	0.00072	5.62
1.2	4.010	0.00084	5.68
1.1	3.327	0.00096	3.61

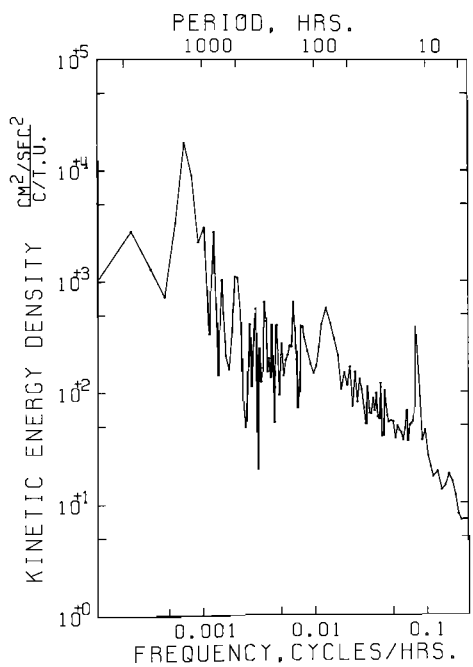

Fig. 11. Autospectrum between speeds in the middle two current meters of the west mooring.

Salt Mixing Coefficient

25°–30°		30°–35°		35°–40°		40°–43°		
$\frac{dS}{dz}\,10^{-10}$ g cm^{-4}	K_s cm^2 s^{-1}	$\frac{dS}{dz}\,10^{-10}$ g cm^{-4}	K_s cm^2 s^{-1}	$\frac{dS}{dz}\,10^{-10}$ g cm^{-4}	K_s cm^2 s^{-1}	$\frac{dS}{dz}\,10^{-10}$ g cm^{-4}	K_s cm^2 s^{-1}	$\bar{K}_s$
3.58	1.584	3.06	1.853	2.00	2.835	2.00	2.835	1.706
3.90	1.487	4.01	1.446	2.76	2.101			1.246
4.06	1.468	4.41	1.351					0.905
2.66	2.071							1.006
								0.639
								0.251
								0.347
								0.341
								0.197
								1.063
3.58	4.969	3.06	5.814	2.00	8.895	2.00	8.895	5.353
3.90	4.900	4.01	4.766	2.76	6.924			4.105
4.06	5.209	4.41	4.796					3.213
2.66	8.323							4.043
								3.107
								1.566
								3.099
								4.027
								2.856
								3.926

from inertial waves. Even a glance at the current meter records show that unanticipated time-dependent surges with a 60-day time scale were responsible for moving most of the water northward.

The nature of the surges bears some inspection. In many of the current meters these surges were separated by periods of slower currents in directions other than north, but in the two records with strongest northward flow only approximately 10 of the 360 days had a negative northward component to the flow. The records also clearly show that the velocity lags the events of cold temperature by some few days. To quantify this lag, a correlation coefficient defined by

$$\sigma_{xy} = \frac{\overline{(x_i - \bar{x})\,(y_i - \bar{y})}}{[\overline{(x_i - \bar{x})^2}]^{1/2}\,[\overline{(y_i - \bar{y})^2}]^{1/2}}$$

was calculated, where x and y can stand for any two quantities. Correlation coefficients for the following pairs of variables were calculated: northward velocity and temperature, eastward velocity and temperature, and, finally, northward velocity and eastward velocity. Table 8 shows the correlation coefficients for these quantities along with the mean quantities of velocity and temperature.

Of course, correlation coefficients by themselves are not too meaningful, but a comparison of the coefficients between the two morrings indicates which side of the current is more disordered. Note the large correlation coefficient between u and v in the top three western current meters. This may represent a large eddy momentum flux which (if down gradient) may create a drag. Because of the sparce nature of the lateral sampling, we cannot quantify this drag with any precision. Note also that northward velocity lags the temperature record by a few days. The correlation coefficients were calculated between v and θ in which v was made to lag θ by 1 day increments for the span of zero to plus 49 days. Table 8 gives the minimum correlation coefficients and their lag times. The east mooring sampled 10, 13, 16, and 20 days time lag, while the west mooring sampled 3, 4, and 5 (twice). For the bottom three moorings, the coefficient was an impressive 0.8 or more.

For the west mooring, the relatively small magnitudes of the correlation between θ and northward velocity (with optimum time lag), and the large value of correlation between u and v indicate that the current may be turbulent and possess substantial eddies. For the east mooring the data are more consistent with a more laminar current whose velocity is strongly correlated with cold events but in which velocity lags the cold events by approximately 4 days. The picture is consistent with a gravity current similar to that studied by *Stern et al.* [1982] but, upside down, surging northward

TABLE 8. Correlation Coefficients Between Pairs of Variables in the Same Current Meter

Mooring	Depth	σ_{uv}	$\sigma_{u\theta}$	$\sigma_{v\theta}$	Minimum $\tau_{v\theta}$ With Time Lag	Days Lag
West	4256	0.771	−0.156	−0.362	−0.688	10
West	4356	0.753	−0.059	−0.094	−0.459	13
West	4406	0.655	0.132	0.170	−0.482	20
West	4446	−0.209	0.418	0.087	−0.474	16
East	4104	0.437	−0.022	−0.446	−0.553	5
East	4204	0.465	−0.407	−0.783	−0.865	4
East	4254	0.509	−0.470	−0.682	−0.795	5
East	4294	0.364	−0.493	−0.755	−0.809	3

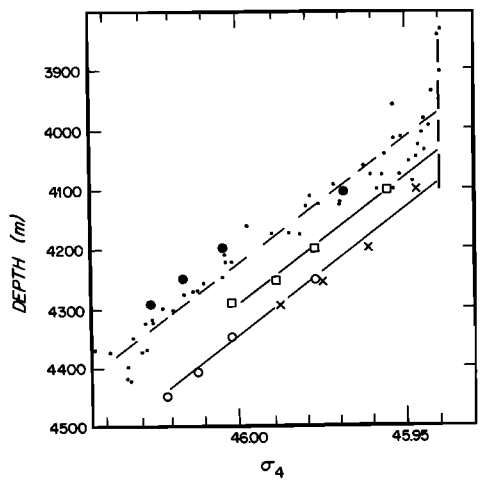

Fig. 12. Sigma-4 versus depth over the Ceara Abyssal Plain (small dots) at the mooring locations. Open circles are from the yearly averaged temperature at the west mooring, and open squares are from the yearly averaged temperatures for the east mooring. The crosses are from temperatures in the east mooring at a slow period (day 246) and the solid circles are from temperatures at the day of fastest flow (day 329).

approximately every 60 days. However, their current was started by removing a barrier. Here it is puzzling what the barrier would correspond to.

The currents are unlike such gravity currents in some ways. There is a unique relation between pressure with respect to the 1.9° isotherm and velocity. To illustrate this, the pressure was calculated by using Figure 12 in which σ_4 is plotted versus depth. The small dots correspond to data taken in stations 66–74 from Nansen casts over the Ceara Abyssal Plain (Figure 6). The errors are believed to be approximately the size of the dots, and the scatter of the dots is due to spatial variability. The squares and circles are values of σ_4 inferred from the 360-day average temperatures from the current meters. σ_4 can be calculated reliably from a temperature record alone because the temperature-salt relationship is extremely tight and linear for these waters (the correlation coefficient in θ and S to a straight line for data deeper than 4000 m in stations 66-74 is 0.99867). One can see that the density surfaces are deeper at 4°N than further south.

Since the relation between σ_4 and depth is relatively linear in Figure 12 (lines have been drawn in by eye), we can calculate pressure by assuming fluid has density of $\sigma_4 = 45.943$ above a depth of $3970 + h$ meters with uniform density gradient $(1/\rho)(\partial\rho/\partial z) = 2.3 \times 10^{-7}$ m^{-1} below. The value of h will be determined by the intersection of the lines drawn through the data in Figure 12 with the vertical dashed line at $\bar{\sigma}_4 = 45.943$. Pressure difference between the 'upstream fluid' (presumed at rest) and downstream fluid at depth ε can be determined by the formula

$$\frac{p}{\rho} = g\frac{\partial\rho}{\partial z}\frac{h(h+2\varepsilon)}{2\rho}$$

(obtained by integrating the hydrostatic equation with the above density distribution). It is well known that a laminar steady current in which friction is negligible has

$$\frac{\rho}{2}v^2 + p = \text{constant}$$

along streamlines even in the presence of frame rotation [*Whitehead et al.*, 1974]. It is useful to calculate this quantity for our current during a maximum and minimum flow period to see how much like a laminar current it is.

For the east mooring, $h = 63$ m and velocity maximum is at 4230 m, so let us select $\varepsilon = 197$ m. With these numbers p/ρ equals 0.032 m^2 s^{-2} while the value of $1/2\ \bar{v}^2$ is 0.0028, more than an order of magnitude less than the pressure. This means the velocity is considerably smaller than the velocity a particle of water would have if it were flowing from the Ceara Abyssal Plain to the 4°N section within a stationary flow with no friction according to Bernoulli's law and with the observed deepening of the time-averaged isotherms.

The pressure-velocity relationships of the fluctuating flows are even more dramatic. Let us look at the relation between pressure and velocity during a large (northward) current event and during a very small current event. To calculate pressure the same procedure was used. The days selected are shown by arrows on Figure 8*a* and the calculated densities for those days are shown in Figure 12. The results are presented in Table 9 for only the east mooring, where the biggest velocities were observed. Because of the high correlation between cold temperature and large velocities, the big surges have pressures far too high compared with those predicted by Bernoulli's law, while the periods with small or zero flow have pressures too low. Some process is therefore taking Bernoulli potential away from the fluid during part of the time and giving it to other fluid. In the extreme case the pressure of the fastest flowing waters was even higher than the upstream (stagnation) pressure.

Are there any candidates for forcing these flows rather than having them driven by their own buoyancy forces? It seems unlikely. Nowhere in the sections do we see any spatial variability of isotherms in excess of 50 m except near the northward flow at 4°N, and near the edge of the Ceara passage. Although we believe the 360-day record was long enough to yield an accurate estimate of the mean flux into the North Atlantic, little is known of the dynamics of the sporadic flow. We are unaware of data sets that would adequately resolve such long period surges elsewhere near oceanic sills.

Speculation as to the mechanism that produces the surge is beyond the scope of this paper. The only oscillating critical flow that we know of is poorly understood and is in a rather different geometry [*Whitehead and Porter*, 1977]. In

TABLE 9. Relation Between Instantaneous Pressure Difference Between Upstream and Mooring and Half the Square of the Instantaneous Speed

	Day	Speed	Depth	Speed^2/2 (cm^2 s^{-2})	h	ε	P/ρ (cm^2 s^{-2})
Maximum speed	329	0.197	(4204)	0.015	−15	+234	+0.008
Minimum speed	246	0.029	(4254)	0.004	120	164	−0.06

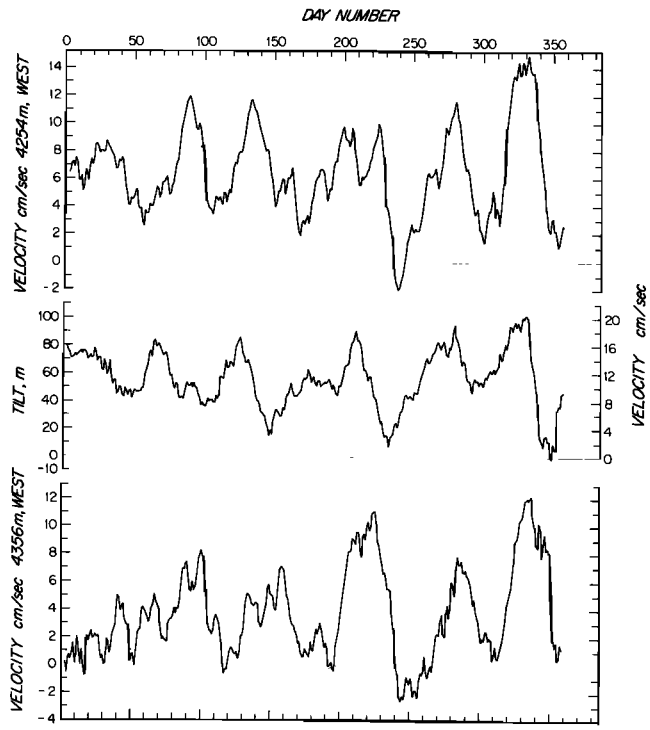

Fig. 13. Plot of tilt of the 1.5°C isotherm and velocity versus time.

that case there was a shallow-water wave which swirled around the upstream basin (which was a flat cylindrical tank) so that the water exiting the tank surged over the edge of the sill (in that case a round hole) as a deep wave with high exit velocities. Possibly a Kelvin wave propagates around the boundaries of the Ceara Abyssal Plain in synchronization with the flushing process. One must do more than invoke drag to make a sensible model of such a surging process since the large surges in current had more energy (kinetic plus potential) than the water probably had upstream and the slow currents had much less.

The pressures calculated above can also be used to test whether the geostrophic relation holds over short periods of time (a few days). Does

$$v = \frac{1}{f}\frac{\delta p}{\delta x}$$

agree with the values obtained by the current meters? Here δ denotes a difference between east and west mooring. Let us pick the same ε for each mooring so to calculate lateral pressure gradient we set

$$\frac{1}{\rho}\frac{\delta p}{\delta x} = \frac{g}{\rho}\frac{\partial \rho}{\partial z}(h + \varepsilon)\frac{\partial h}{\partial x}$$

Taking an average of h as 90 m, (since $\varepsilon > h$ we set h constant) $\varepsilon = 260$ m, $(g/\rho)(\partial\rho/\partial z) = 2.3 \times 10^{-7}$ and values of tilt of the isotherms from the records of the current meters, we predict that $v \equiv 8.05\,(\partial h/\partial x) = 0.00197\,\delta h$ m s^{-1} where δh is tilt of isotherms in meters. Figure 13 shows tilt of a 5-day running mean of the 1.5° isotherm and velocities from one current meter from each mooring. The running mean was taken to eliminate the three day oscillation which is almost certainly not geostrophic. A high correlation between tilt and velocity is clearly evident. On the left is a scale of velocity as given by $v = 0.00197\,\delta h$ (from above). The observed velocities of the east mooring agree to within 40% while the observed velocities of the west mooring agree to within 60%. The picture is therefore consistent with large flows occurring during sharply tilting, cold water events. When flows were slow, there was less tilt, and isotherms were deeper. Therefore, the isotherms were more sharply tilted somewhere to the east during those periods. It is unknown whether there was a large mass flux east of our array during those periods.

How big is the mass flux when compared with some of the simplest hydraulic control problems? Let us first test whether the formula

$$Q = \frac{g h_u^2}{2f}$$

gives good results where h_u is height of the dense fluid above the sill in the upstream basin. If we take the continuously stratified fluid equivalent to a two layer fluid by the substitution $g^* = g\,\partial\rho/\partial z\; h/2 = N^2 h_u/2$ we have

$$Q = \frac{N^2 h_u^3}{4f}$$

which, for $h_u = 400$ m, $N = 0.0015$, and $f = 10^{-5}$ predicts

$$Q = 3.6 \times 10^6 \text{ m}^3/\text{s}^{-1}$$

The value of h_u we should pick, however, is unclear and a value of $h_u = 300$ m gives $Q = 1.5 \times 10^6$, a value between our current meter and geostrophic estimates. Rydberg advocates the formula

$$Q = \frac{2}{9}\frac{g' h_u^2}{f}$$

for a rectangular basin. This gives volume flux of 1.6×10^6 m^3 s^{-1} for $h_u = 400$ m and $.67 \times 10^6$ m^3 s^{-1} for $h_u = 300$ m. The former is in good agreement and the latter is probably too small. We conclude that the simple hydraulic models predict the approximate correct flux, but scatter due to uncertainty in the upstream conditions and the applicability of a continuously stratified fluid to a two-layer problem is as big as scatter due to the disagreement between the two measuring methods.

The observations seem to differ from abyssal circulation models. *Stommel and Arons* [1972] have modeled the northward flowing current as an inertial current with small shear that leans against the western slope. A major change on the depth of the western boundary current is predicted to occur between 3°S and the equator. Our southernmost section shows little evidence for an inertial current, and a detailed model of the dynamics of the current as it makes its way over the abyssal plain is beyond the resolution of the data set. The first evidence of an inertial current is in the dogleg below the Ceara Rise, where there is a tilt of the isotherms into the rise. The problem of how the fluid crosses the equator remains open.

Acknowledgments. Support was given for this study from the Ocean Sciences Division, National Science Foundation, under grant OCE 77-7507. Woods Hole Oceanographic contribution number 4855. We are indebted to Lorraine Barbour and the Buoy Group's analysis section for careful handling of the data and the Buoy Group in general for skillful deployment and retrieval of the current meters with 100 percent successful sampling. We also thank Raymond W. Schmitt for his helpful suggestions on diffusion coefficients.

REFERENCES

Bryden, H. L., Geostrophic vorticity balance in midocean, *J. Geophys. Res., 85,* 2825–2828, 1980.

Clarke, R. A., H. W. Hill, R. F. Reiniger, and B. A. Warren, Current system south and east of the Grand Banks of Newfoundland, *J. Phys. Oceanog., 10,* 25–65, 1980.

Eriksen, C. C. Observations of internal wave reflection off sloping bottoms, *J. Geophys. Res., 87,* 525–538, 1982.

Gill, A. E., The hydraulics of rotating-channel flow, *J. Fluid Mech., 80,* 641–670, 1977.

Hogg, N. G., P. Biscaye, W. Gardner, and W. J. Schmitz, Jr., On the transport and modification of Antarctic Bottom water in the Vema Channel, *J. Mar. Res., 40* (suppl.), in press, 1981.

Mantyla, A. W., Electrical conductivity comparisons of Standard Seawater batches p29 to p84, *Deep Sea Res., 27A,* 837–846, 1980.

McCartney, M. S., L. V. Worthington, and M. E. Raymer, Anomalous water mass distributions at 55W in the North Atlantic in 1977, *J. Mar. Res., 38,* 147–172, 1980.

Moody, R., D. E. Hayes, and S. Connary, Bathymetry of the continental margin of Brazil, *Map number 832,* Am. Assoc. Petrol. Geol., Tulsa, Okla., 1979.

Rydberg, L., Rotating hydraulics in deep-water channel flow, *Tellus, 32,* 77–89, 1980.

Sclater, J.G., C. Jaupart, and D. Galson, The heat flow through oceanic and continental crust and the heat loss of the equator, *Rev. Geophys. Space Phys., 18,* 269–311, 1980.

Stern, M. E., J. A. Whitehead, Jr., and B. L. Hua, The intrusion of a density current along the coast of a rotating fluid, *J. Fluid Mech.,* in press, 1982.

Stommel, H., The abyssal circulation, *Deep Sea Res., 5,* 80–82, 1958.

Stommel, H., and A. B. Arons, On the abyssal circulation of the world ocean, 5, The influence of bottom slope on the broadening of inertial boundary currents, *Deep Sea Res., 19,* 707–718, 1972.

Veronis, G., Use of tracers in circulation studies, in *The Sea,* vol. 6, edited by E. D. Goldberg, pp. 169–188, John Wiley, New York, 1977.

Whitehead, J. A., Jr., A. Leetmaa, and R. A. Knox, Rotating hydraulics of strait and sill flows, *Geophys. Fluid Dyn., 6,* 101–125, 1974.

Whitehead, J. A., Jr., and D. L. Porter, Axisymmetric critical withdrawal of a rotating fluid, *Dyn. Atmos. Oceans, 2,* 1–18, 1977.

Whitehead, J. A., Jr., Rotating critical flows in the ocean, in *Proceedings Second International Symposium on Stratified Fluids,* edited by T. Carstens and T. McClimans, Tapir, Trondheim, 1980.

Worthington, L. V., *On the North Atlantic Circulation, Oceanogr. Stud.,* vol. 6, The Johns Hopkins University Press, Baltimore, Maryland, 1976.

Worthington, L. V., The water masses of the world ocean: some results of a fine-scale census, 1, in *Evolution of Physical Oceanography,* edited by B. A. Warren and C. Wunsch, pp. 42–69, MIT Press, Cambridge, Massachusetts, 1981.

Worthington, L.V., and W. G. Metcalf, The relationship between potential temperature and salinity in deep Atlantic water, *Rapp. Cons. Explor. Mer., 149,* 122–128, 1961.

Worthington, L. V., and W. R. Wright, North Atlantic Ocean Atlas of potential temperature, salinity and oxygen profiles from the *Erika Dan* cruise of 1962, report, Woods Hole Oceanogr. Inst., Woods Hole, Mass., 1970.

Wright, W. R., and L. V. Worthington, The water masses of the North Atlantic Ocean—A volumetric census of temperature and salinity, *Serial Atlas of the Marine Environment,* Folio 19, American Geographic Society, Milwaukee, Wis., 1970.

Wüst, G., The stratosphere of the Atlantic Ocean (1935), Amerind, New Delhi, 1978.

(Received April 17, 1981;
revised May 12, 1982;
accepted May 12, 1982.)